Dalton Transactions

ROYAL SOCIETY OF CHEMISTRY

PAPER

View Article Online
View Journal | View Issue

Cite this: *Dalton Trans.*, 2026, **55**, 476

Heterolytic cleavage of the B–H bond in $H_3B{\cdot}L$ (L = THF, NMe_2H) by an electrophilic Ir(III) pincer complex [Ir(H)(PMe_3)(^{tBu4}POCOP)][BAr^F_4]

Mitarani Pradhan, [a] Zeel Y. Surati, [b,c] Apurba Kumar Pal,[a] Kumar Vanka *[b,c] and Balaji R. Jagirdar *[a]

Six- and five-coordinate iridium complexes, [Ir(H)Cl(PMe_3)(^{tBu4}POCOP)] (**2**) (^{tBu4}POCOP = κ^3-C_6H_3-2,6-(OP^tBu_2)$_2$) and [Ir(H)(PMe_3)(^{tBu4}POCOP)][BAr^F_4] (**3**), respectively, have been synthesized and characterized. The reactivity of the electrophilic 16-electron iridium(III) complex **3** with H_2, $H_3B{\cdot}THF$, $H_3B{\cdot}NMe_2H$, and $H_3B{\cdot}NMe_3$ was investigated. The reaction of complex **3** with H_2 resulted in the formation of *trans*-[Ir(H)(η^2-H_2)(PMe_3)(^{tBu4}POCOP)][BAr^F_4] complex **5**. Complex **3** was found to activate the B–H bonds in $H_3B{\cdot}THF$ and $H_3B{\cdot}NMe_2H$ (DMAB) in a heterolytic fashion. The reaction of complex **3** with $H_3B{\cdot}THF$ at 298 K afforded *trans*-[Ir(H)$_2$$PMe_3$(^{tBu4}POCOP)] complex **6** and a boronium compound, [$H_2B(THF)_2$][BAr^F_4]. Monitoring the reaction from 179 to 298 K by NMR spectroscopy revealed the formation of a σ-borane intermediate, *trans*-[Ir(H)(η^1-$HBH_2{\cdot}THF$)PMe_3(^{tBu4}POCOP)][BAr^F_4] (**3a-Int**), *en route* to the final products observed at 298 K. The formation of this intermediate species was also investigated by density functional theory (DFT) calculations. The reaction of complex **3** with $H_3B{\cdot}NMe_2H$ at 298 K yielded a mixture of complexes **3** and **5** and a cyclic diborazane [H_2BNMe_2]$_2$. The reaction was found to proceed *via* intermediates, a σ-borane complex, *trans*-[Ir(H)(η^1-$HBH_2{\cdot}NMe_2H$)PMe_3(^{tBu4}POCOP)][BAr^F_4] (**3b**), complex **6**, [$(NHMe_2)_2BH_2$][BAr^F_4], and $H_2B{=}NMe_2$. Complex **3** exhibited no reactivity with $H_3B{\cdot}NMe_3$.

Received 26th July 2025,
Accepted 24th November 2025

DOI: 10.1039/d5dt01780g

rsc.li/dalton

Introduction

Transition metal σ-borane complexes that involve binding of the B–H bond to metal centers, resulting in a 3c–2e bonding interaction, are well-known reactive intermediates in several catalytic processes.[1–3] They include hydroboration of alkenes and alkynes,[4,5] dehydrogenation of amine–boranes,[6–10] and borylation of C–H bonds.[11] In σ-borane complexes, boranes ($H_3B{\cdot}L$; L = THF, NRR′R″ (R, R′, R″ = H, alkyl)) exhibit various binding modes such as η^1,[12–17] η^2,[18,19] and K^2.[13,20–22] Additionally, catalytic dehydrocoupling reactions of amine–boranes, which result in the evolution of large quantities of H_2, have attracted significant interest; in particular, ammonia–borane, with its large hydrogen content, is quite promising for hydrogen storage applications. Furthermore, in these reactions, B–N bond formation results, which has applications in the synthesis of oligomeric and polymeric materials containing B–N and B=N bonds.[6,23–25]

Amine boranes have emerged as versatile substrates for transition metal-catalyzed B–H bond activation, typically proceeding through either dehydrocoupling or dehydrogenative homocoupling pathways. Both pathways involve the formation of a key σ-borane complex intermediate prior to B–H bond cleavage. In the case of primary and secondary amine boranes such as $H_3B{\cdot}NH_3$,[23,26] $H_3B{\cdot}NMeH_2$,[14] and $H_3B{\cdot}NMe_2H$,[27] the presence of an N–H proton facilitates dehydrocoupling to yield $H_2B{=}NRR'$ (R, R′ = H, Me) along with the release of H_2. These amino–borane species can subsequently undergo cyclization to form cyclic dimers [H_2BNRR']$_2$. In contrast, tertiary amine boranes like $H_3B{\cdot}NMe_3$, where no N–H proton is available, two molecules coordinate to the metal center and undergo dehydrogenative homocoupling.[13] This results in the formation of B–B bonded amine–borane dimers $(BH_2{\cdot}NMe_3)_2$ along with H_2 evolution. In certain σ-borane complexes, H/D exchange takes place between metal hydride and the coordinated B–D bond of amine–borane ($H–M–D–BD_2{\cdot}NMe_3$).[28]

Unlike the amine boranes, $H_3B{\cdot}THF$ exhibits different reactivity patterns with transition metal complexes. One such reactivity involves the formation of borohydride complexes through its reactions with metal hydride and σ-dihydrogen complexes. For example, the reaction of $H_3B{\cdot}THF$ with a series of Ni(II) hydride complexes, [Ni(H)(pincer)] {pincer = ^{R4}POCOP;[29] POCOP = 2,6-$C_6H_3(OPR_2)_2$, R = ^{t}Bu, ^{i}Pr, cyclopentyl and pincer = PCP^{Me}-iPr = 2,6-$C_6H_3(N^{Me}{-}P^{iPr2})_2$}[30] afforded the corresponding Ni(II) borohydride complexes, [Ni(BH_4)(pincer)] (Fig. 1A-(i)). The reaction

[a]*Department of Inorganic and Physical Chemistry, Indian Institute of Science, Bengaluru 560012, India. E-mail: jagirdar@iisc.ac.in*
[b]*Physical and Materials Chemistry Division, CSIR-National Chemical Laboratory, Pune 411 008, India*
[c]*Academy of Scientific and Innovative Research (AcSIR), Ghaziabad 201 002, India*

of $H_3B{\cdot}THF$ with a Rh(I) σ-H_2 complex, [Rh(η²-H_2)(^{tBu4}(PNCNP)] {^{tBu4}(PNCNP) = 2,6-C_6H_3(NHP^tBu_2)$_2$} afforded the corresponding Rh(III) hydrido borohydride complex, [Rh(H)(κ²-BH_4)(^{tBu4}(PNCNP)] (Fig. 1A-(ii)).[31] An additional reactivity involves the insertion of a BH_3 moiety into a M–C bond. For example, BH_3 was inserted into Co–C(benzyl) in [Co(Imes′)(SiHPh-Imes′)] {Imes′ = cyclometalated 1,3-dimesitylimidazol-2-ylide; SiHPh-Imes′ = silylated Imes′} and [Cp*Co(2-$C_6H_4PPh_2$)] complexes, forming aryl borohydride complexes, [Co(κ²-H_2BH-Imes′)(SiHPh-Imes′)] and [Cp*Co(κ³-H,H,P-$H_3BC_6H_4PPh_2$)], respectively (Fig. 1B).[32,33] A further reaction involves the coordination of BH_3 to metal centers forming an η²-BH_3 σ-borane complex. For example, [Ru(H)$_2$(BH_3)(Me-PNP)][19] (Me-PNP = ^{Me}N-($CH_2CH_2P^{tBu2}$)$_2$) and [(^{tBu}POCOP)IrH_2(BH_3)][18] σ-borane complexes formed from [Ru(H_2)(H)$_2$(Me-PNP)] and [(^{tBu}POCOP)IrH_2] complexes, respectively (Fig. 1C).

Herein, we report a heterolytic cleavage of the B–H bond in $H_3B{\cdot}THF$ by a cationic Ir(III) pincer complex, [Ir(H)(PMe_3)(^{tBu4}POCOP)][BAr^F_4] (**3**) (^{tBu4}POCOP = κ³-C_6H_3-2,6-(OP^{t}Bu$_2$)$_2$). This reaction results in the formation of a neutral dihydride complex, *trans*-[Ir(H)$_2$(PMe_3)(^{tBu4}POCOP)] (**6**), along with the [H_2B(THF)$_2$][BAr^F_4] adduct (Fig. 1D). The activation of the B–H bond in $H_3B{\cdot}THF$ proceeds *via* the formation of a σ-borane complex, *trans*-[Ir(H)(η¹-$HBH_2{\cdot}THF$)PMe_3(^{tBu4}POCOP)][BAr^F_4] (**3a-Int**), which was observed at low temperature. Additionally, we have studied heterolytic cleavage of the B–H bond in $H_3B{\cdot}NMe_2H$ as well. The results of these studies have been presented herein.

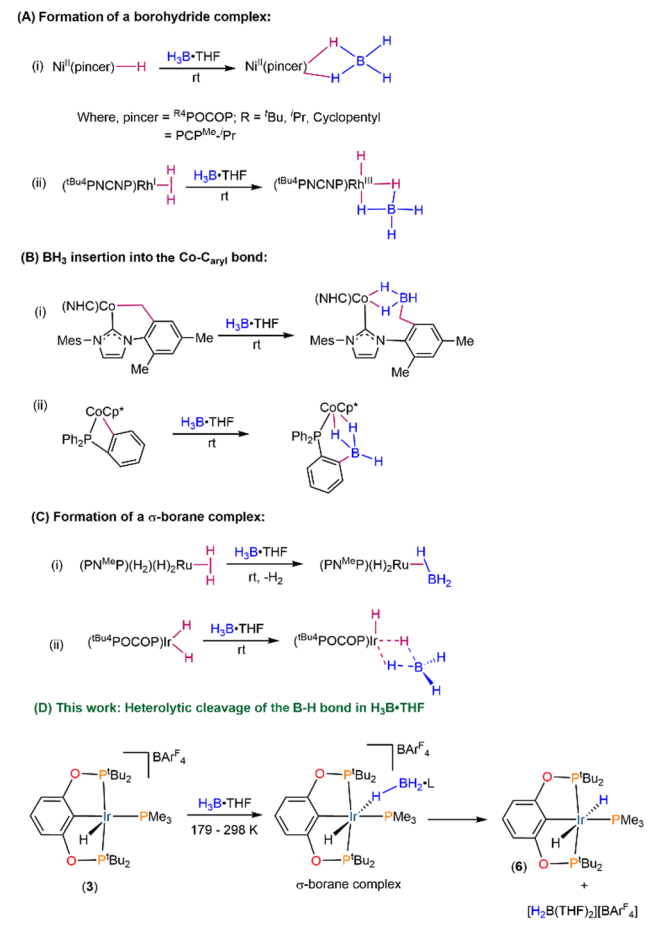

Fig. 1 Different reactions of $H_3B{\cdot}THF$ with transition metal complexes. (A) Formation of a borohydride complex; (B) BH_3 insertion into a Co–C_{aryl} bond; (C) formation of a σ-borane complex; and (D) our work: heterolytic cleavage of the B–H bond in $H_3B{\cdot}THF$.

Results and discussion

Synthesis and characterization of [Ir(H)(PMe_3)(^{tBu4}POCOP)][BAr^F_4] (3)

The reaction of the five-coordinate, 16-electron Ir(III) hydride chloride complex, [Ir(H)Cl(^{tBu4}POCOP)] (**1**) (^{tBu4}POCOP = κ³-C_6H_3-2,6-(OP^{t}Bu$_2$)$_2$), with 1.0 equiv. of PMe_3 instantaneously afforded the six-coordinate, 18-electron Ir(III) complex, [Ir(H)Cl(PMe_3)(^{tBu4}POCOP)] (**2**) (eqn (1)). Formation of complex **2** was established by NMR spectroscopy (Fig. S1–S4). The hydride in complex **2** appeared as a triplet of doublets at −22.32 ppm due to coupling with two *cis*-phosphorus, followed by coupling with PMe_3 ($^2J_{H,Pin}$ = 14.4 Hz and $^2J_{H,PMe3}$ = 11.6 Hz), in the ^{1}H NMR spectrum. This chemical shift value is in accordance with a previously reported value of −21.52 ppm for the hydride in the complex [Ir(H)Cl(PPh_3)(^{iPr4}POCOP)] (^{iPr4}POCOP = κ³-C_6H_3-2,6-(OP^{i}Pr$_2$)$_2$).[34]

(1)

Soon after complex **2** was formed, the chloride ligand was abstracted using $NaBAr^F_4$. This resulted in the formation of a five-coordinate, 16-electron Ir(III) complex, [Ir(H)(PMe_3)(^{tBu4}POCOP)][BAr^F_4] (**3**) (Scheme 1). Complex **3** could be isolated in the solid state. In the ^{1}H NMR spectrum, a doublet of triplets appeared at −42.46 ppm ($^2J_{H,PMe3}$ = 20.0 Hz, $^2J_{H,Pin}$ = 10.0 Hz) for the hydride in complex **3** (Fig. S12). The large upfield shifted signal in the hydride region for complex **3** is indicative of a hydride ligand *trans* to a vacant site.[35,36] Variable-temperature NMR spectral studies of complex **3** in CD_2Cl_2 were conducted (Fig. S19–S22). The hydride signal was found to be invariant with respect to temperature. However, in the reported 16-electron Ir(III) complexes, [Ir(H)(L)(^{iPr4}POCOP)][BAr^F_4] (L = PPh_3, $PMePh_2$, PMe_2Ph), the sixth-coordination site is occupied by a weakly bound solvent or an N_2 molecule.[37] The molecular structure of complex **3** was established by an X-ray diffraction study. Crystals were grown by slow vapor diffusion of *n*-pentane into a saturated CH_2Cl_2 solution of complex **3** at ambient temperature. The ORTEP view (Fig. 2) shows that complex **3** exhibits a distorted square pyramidal geometry. The hydride position was located from the difference Fourier map, and the Ir–H bond length was found to be 1.25(6) Å. A similar five-coordinate cationic complex, [Ir(H)(CO)(^{tBu4}POCOP)][BAr^F_4], has been reported with a CO ligand in place of PMe_3, featuring an Ir–H bond length of 1.58(7) Å.[38]

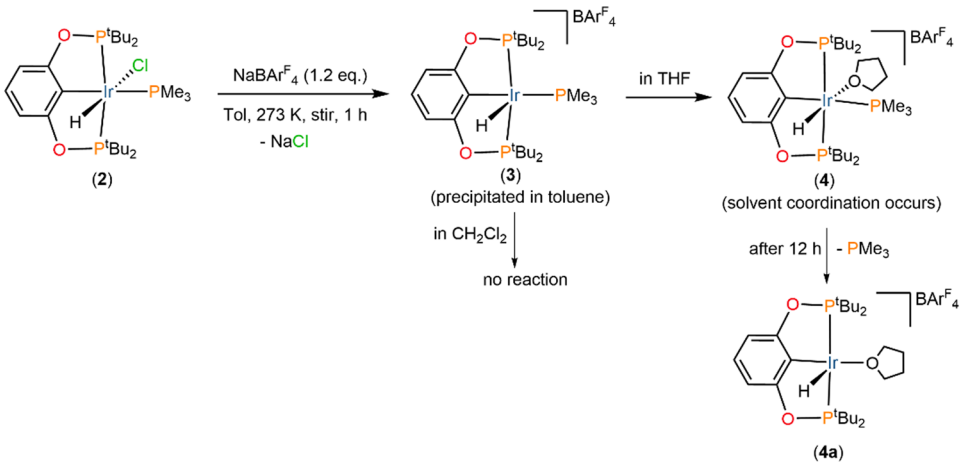

Scheme 1 Synthesis of the [Ir(H)(PMe$_3$)(^{tBu4}POCOP)][BAr$^F_4$] complex (**3**) and its reactivity with THF and CH_2Cl_2.

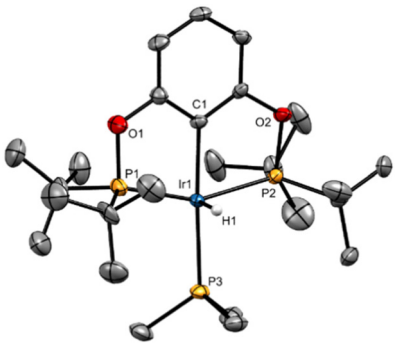

Fig. 2 ORTEP view of complex [Ir(H)(PMe$_3$)(^{tBu4}POCOP)]$^+$ (**3**) (50% thermal ellipsoidal probability). Counter anions and non-hydride H atoms have been omitted for clarity. Only the major component of the disorder is shown for clarity. Selected bond lengths (Å) and bond angles (°): Ir1–H1, 1.25(6); Ir1–P1, 2.3235(9); Ir1–P2, 2.3425(8); Ir1–P3, 2.3717(8); Ir1–C1, 2.054(3); and P1–Ir1–P2, 156.13(3); C1–Ir1–P3, 175.79(8).

In THF solvent, the hydride signal at −42.46 ppm in complex **3** disappeared, and a new broad signal appeared at −22.38 ppm (Fig. S25), which is indicative of the coordination of THF at the sixth coordination site of the metal (Scheme 1). This interaction results in the formation of a six-coordinate, 18-electron Ir(III) complex, [Ir(H)(THF)(PMe$_3$)(^{tBu4}POCOP)][BAr$^F_4$] (**4a**). In the ^{1}H NMR spectrum, the hydride ligand of this species appears as a triplet ($^2J_{H,P(cis)}$ = 12.0 Hz) at −40.94 ppm (Fig. S30). A similar complex with a different counter anion, [Ir(H)(acetone)(^{tBu4}POCOP)][B(C$_6$F$_5$)$_4$], was previously reported by Brookhart and co-workers, where the hydride peak was observed at −42.28 ppm as a triplet ($^2J_{H,P(cis)}$ = 12.4 Hz).[39] Notably, the formation of phosphine oxide, as evidenced in the NMR spectra (Fig. S34 and S35), is most likely the driving force for the partial dissociation of PMe$_3$.

Reaction of the [Ir(H)(PMe$_3$)(^{tBu4}POCOP)][BAr$^F_4$] complex (3) with H$_2$

Since complex **3** has a vacant sixth coordination site, H_2 (1.0 bar) was introduced into a CD_2Cl_2 solution of the complex at 298 K (eqn (2)). The reaction was monitored by variable-temperature (VT) NMR spectroscopy (Fig. S36–S44) over a temperature range of 298–178 K. Fig. 3 shows a VT NMR spectral stack plot, illustrating the progression of the reaction of complex **3** with H_2.

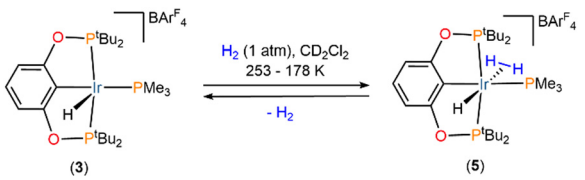

(2)

At 298 K, in the ^{1}H NMR spectrum, a doublet of triplets at −42.46 ppm was observed for the Ir–H in complex **3**. Upon introduction of H_2, a very broad signal appeared at −37.37 ppm corresponding to the Ir–H in the *trans*-[Ir(H)(η^2-H$_2$)(PMe$_3$)(^{tBu4}POCOP)][BAr$^F_4$] complex (**5**), while the signal for free H_2 was found to be slightly upfield shifted from 4.60 to 3.33 ppm in the ^{1}H NMR spectrum (Fig. S38). Upon cooling the reaction mixture to 253 K, the broad peaks at −37.37 and 3.33 ppm disappeared and two new broad signals appeared at −3.69 and −14.61 ppm. These signals could be assigned to the bound H_2 and the Ir–H in complex **5**. Further cooling to 183 K resulted in a broad signal at −14.61 ppm due to the Ir–H getting resolved into a quartet {J(H,P$_{cis}$) = 14.0 Hz, coupling with the three *cis*-phosphorus nuclei}, while the intensity of the signal at −3.69 ppm for the bound H_2 increased along with the appearance of a singlet at 4.60 ppm for free H_2. The integral ratio of the signals at −14.61 and −3.69 ppm was found to be 1 : 2 at 183 K. The signals of the σ-H_2 complex **5** are observable from 253 to 178 K. These temperature-dependent spectral variations suggest that the binding of H_2 to the iridium center in complex **3** is weak at 298 K, resulting in an exchange involving binding and lability of H_2 (eqn (2)). At low temperatures,

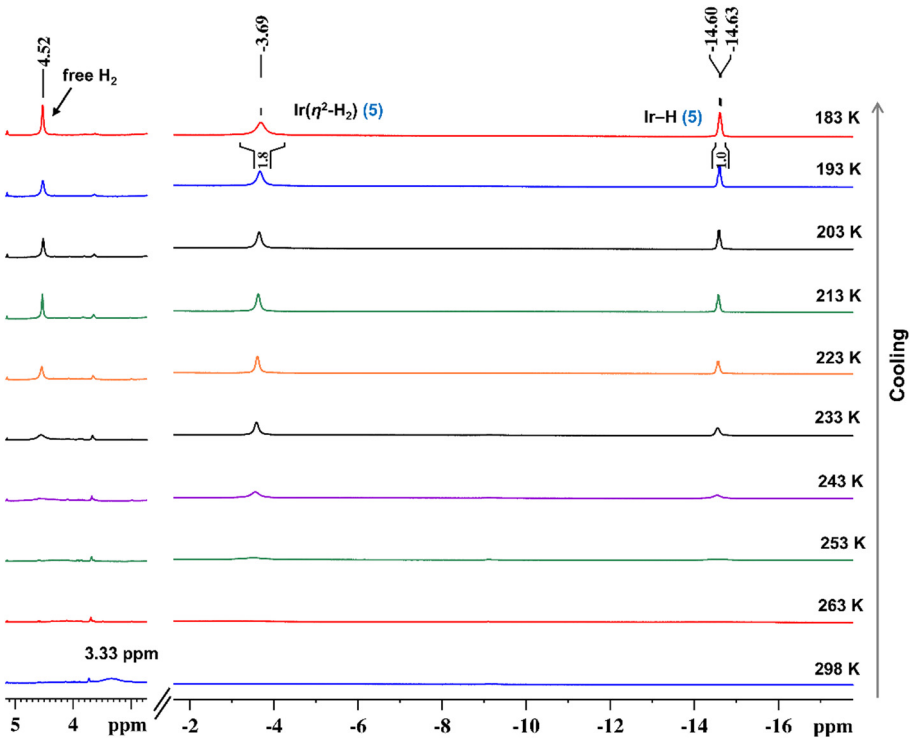

Fig. 3 Partial VT ^{1}H NMR (500.0 MHz, CD_2Cl_2) spectral stack plot of the reaction of [Ir(H)(PMe_3)(^{tBu4}POCOP)][BAr^F_4] (**3**) with H_2.

the exchange rate is slow, leading to the formation of complex **5**.

In the $^{31}P\{^{1}H\}$ NMR spectrum as well, two broad signals appeared at 178.8 and −43.8 ppm due to the exchange and these two signals could be assigned to the pincer phosphines and PMe_3 ligand, respectively (Fig. S41). Similar examples of reactions of cationic five-coordinate complexes with PPh_3 and CO ligands in place of PMe_3 have been reported. In the case of the PPh_3 analogue, [Ir(H)(PPh_3)(^{iPr4}POCOP)]$^+$,[37] H_2 binds to form the *trans*-H_2/hydride complex at 253 K at a H_2 pressure of 1.0 bar. In contrast, in the case of CO analogues, [Ir(H)(CO)(^{iPr4}POCOP)]$^+$,[40] [Ir(H)(CO)($^{(NMe2)(tBu4)}$POCOP)]$^+$ ($^{(NMe2)(tBu4)}$POCOP = κ^3-$NMe_2C_6H_3$-2,6-(OP^tBu_2)$_2$),[41] and [Ir(H)(CO)(^{tBu4}POCOP)]$^+$,[42] no reactions were noted with H_2 under these mild reaction conditions.

The VT ^{1}H NMR spin–lattice relaxation time (T_1, ms; 500 MHz) measurements were carried out for the *trans*-[Ir(H)(η^2-H_2)(PMe_3)(^{tBu4}POCOP)][BAr^F_4] complex (**5**) at 10 K intervals (Table S1). The T_1(min, 500 MHz) of the broad signal at −3.69 ppm was found to be 15.64 ms at 207 K (Fig. S42). The short T_1(min) value indicates that the H–H bond in the bound H_2 ligand is intact. To support the assignment further, the HD isotopomer, *trans*-[Ir(H)(η^2-HD)(PMe_3)(^{tBu4}POCOP)][BAr^F_4] (**5-HD**), was prepared by introducing *in situ* generated HD gas to complex **3**. At 213 K, complex **5-HD** displayed a multiplet at −3.64 ppm which is comprised of peaks of the bound HD and H_2 (Fig. 4a). Upon suppressing the peak of the bound H_2, we obtained a six-line pattern or two 1 : 1 : 1 triplets closely spaced from each other. It is considered that adjacent lines of this pattern equate to 16.5 and 16.8 Hz, whereas alternate lines equate to 33.0 and 33.5 Hz (Fig. 4a). These values could be treated as $^{1}J_{H,D}$ coupling constants of H–D isotopologues. The d_{H-H} values of the bound H_2 could be calculated to be 0.869 and 0.861 (Å).[1]

The assignment of doublets of triplets could be ruled out since the bound H_2 in complex **5** displayed only a broad singlet, indicating that it couples neither with the *trans* hydride nor any of the three *cis*-^{31}P nuclei (two $^{31}P_{pincer}$ and one $^{31}P_{PMe3}$). Upon decoupling of ^{31}P, the ^{1}H NMR spectrum of complex **5-HD**, with the multiplet containing six lines, remained unchanged (Fig. S49). In order to decipher the structural formulation of the isotopologue(s), we considered different possibilities.

A signal for Ir–D was not observed in the ^{2}H NMR spectrum (Fig. S50), which rules out H/D exchange between Ir–H and Ir (σ-HD). Additionally, Ir–H signal intensity remained unchanged, which once again rules out the formation of *trans*-[Ir(D)(η^2-HD)(PMe_3)(^{tBu4}POCOP)][BAr^F_4]. Chaudret[43] and Moise[44] groups reported the *exo* and *endo* isomers of HD σ-complexes, [$Cp_2Ta(HD)(CO)$]$^+$ and [$Cp'_2Nb(HD)(PMe_2Ph)$]CF_3CO_2, respectively. These isomers exhibited two well-separated triplets with an intensity ratio of 1 : 1 : 1. Based on these considerations, we conclude that this interesting six-line pattern or two closely spaced 1 : 1 : 1 triplets is a manifestation of the presence of two isomers. The poor and/or lack of reasonable signal intensities for the isotopologues, which are observable only at low temperatures, in the ^{2}H NMR spectrum posed challenges to decipher the exact structural formulation

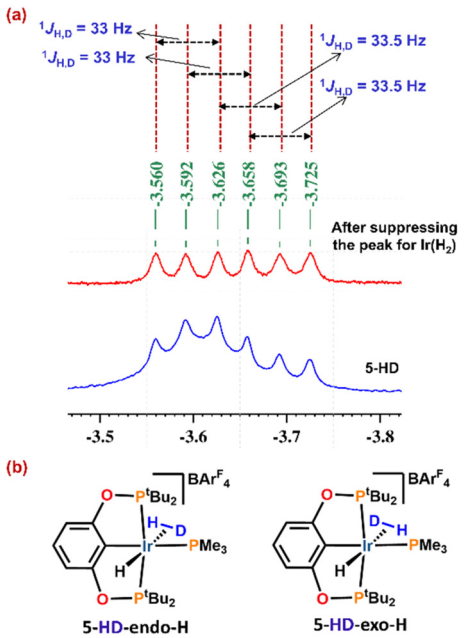

Fig. 4 (a) Partial ^{1}H NMR (500.0 MHz, CD_2Cl_2, 213 K) spectral stack plot (hydride region) of [Ir(H)(η^2-HD)(PMe_3)(^{tBu4}POCOP)][BAr^F_4] (**5-HD**), formed upon purging HD gas through a solution of complex **3** (bottom) and **5-HD** after suppressing the singlet for Ir(H_2) (top). (b) Structure of *endo* and *exo* isomers of complex **5-HD**.

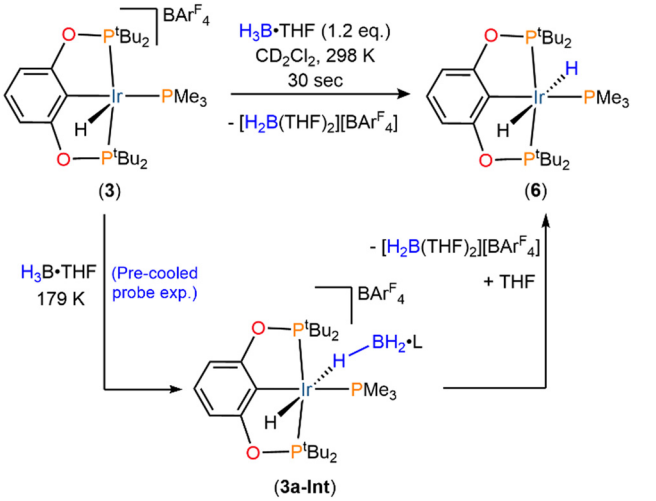

Scheme 2 Reaction of [Ir(H)(PMe_3)(^{tBu4}POCOP)][BAr^F_4] (**3**) with H_3B·THF: formation of the *trans*-[Ir(H)$_2$$PMe_3$(^{tBu4}POCOP)] (**6**) complex.

of these isotopologues. We, therefore, tentatively assign the observed spectral feature to the isomers shown in Fig. 4b.

Reaction of the [Ir(H)(PMe_3)(^{tBu4}POCOP)][BAr^F_4] complex (3) with H_3B·THF

The reaction of complex **3** with 1.2 equiv. of H_3B·THF in CD_2Cl_2 was initially monitored by NMR spectroscopy. It led to the formation of a *trans*-[Ir(H)$_2$$PMe_3$(^{tBu4}POCOP)] complex (**6**) at room temperature (298 K) accompanied by the formation of [$H_2B(THF)_2$][BAr^F_4] and H_2 (Scheme 2). In the ^{1}H NMR spectrum, a distinct quartet was observed at −11.63 ppm, with a $^2J_{H,P(cis)}$ coupling constant of 15.0 Hz and an integral value of two, which could be assigned to the two hydrides in complex **6**. The NMR spectral features of complex **6** are comparable to those of a reported one for the PPh_3 analogue, *trans*-[Ir(H)$_2$$PPh_3$(^{tBu4}POCOP)], by Findlater and co-workers.[45] In the ^{11}B NMR spectrum, a broad triplet was noted at 9.3 ppm ($^1J_{B,H}$ = 130.5 Hz), which could be assigned to [$H_2B(THF)_2$][BAr^F_4]. These data are consistent with the chemical shifts and coupling constants reported for $[H_2B{\cdot}L_2]^+$ (L = NH_2Me, $NHMe_2$) cations.[46,47] The NMR spectral features suggest that the B–H bond in H_3B·THF undergoes heterolytic cleavage to provide a hydride to the iridium metal center, with the boronium compound, [$H_2B(THF)_2$][BAr^F_4], formed as a byproduct.

As the B–H bond cleaves rapidly at room temperature to form complex **6** instantaneously, the reaction was carried out at 179 K. The reaction progress was monitored as a function of temperature (warming gradually to 298 K) using NMR spectroscopy in order to obtain mechanistic insights into this reaction (Fig. 5).

To a frozen CD_2Cl_2 solution of complex **3** held in a liquid N_2 bath, a CD_2Cl_2 solution containing 1.2 equiv. of H_3B·THF was added. The reaction mixture was then transferred to an NMR probe which was pre-cooled to 179 K. As the sample was gradually warmed, the ^{1}H, ^{31}P{^{1}H} and ^{11}B NMR spectral data were acquired (Fig. S63–S75). At 179 K, the ^{1}H NMR spectrum was comprised of a broad singlet at −9.35 ppm, which could be assigned to the bridging B–H bound to the iridium center, and a quartet at −22.8 ppm corresponding to Ir–H (Fig. 5). Based on these spectral features, we formulate this species as a σ-borane complex, *trans*-[Ir(H)(η^1-HBH_2·THF)PMe_3(^{tBu4}POCOP)][BAr^F_4] (**3a-Int**) (Scheme 2). The chemical shift values of complex **3a-Int** are in accordance with those of a similar σ-borane complex, [Ir(^{i}Pr-PN^HP)(H)$_2$($H_3B{\cdot}NMe_3$)][BAr^F_4] (iPr-PN^HP = κ^3-$(CH_2CH_2P^iPr_2)_2NH$).[14] The ^{1}H–^{1}H COSY spectrum (Fig. S69) further confirmed that the signal at −9.35 ppm correlated with an off-diagonal cross peak at 1.93 ppm. The integration ratio of these two peaks is 1 : 2 (Fig. S70 and S71), indicating that the signals at −9.35 and 1.93 ppm are for the B–H_{bridge} and B–$H_{terminal}$ hydrogen atoms, respectively, of the coordinated borane in complex **3a-Int**. On the other hand, due to the typical ^{11}B NMR spectral broadening at low temperatures, peaks of the bound H_3B·THF in complex **3a-Int** and [$H_2B(THF)_2$][BAr^F_4] were not observed at 179 K (Fig. S74). A similar observation was made wherein the signal of the bound $H_3B{\cdot}NHMe_2$ in the σ-borane complex, [RuCl(η^1-$HBH_2{\cdot}NMe_2H$)(dppe)$_2$][OTf] (dppe = $Ph_2PCH_2CH_2PPh_2$),[26] was not observed in the ^{11}B NMR spectrum at low temperatures. In the ^{31}P{^{1}H} NMR spectrum (Fig. S73), two signals were noted at 169.5 and −56.7 ppm for the pincer and PMe_3 ligand, respectively, for **3a-Int**.

In addition to this set of peaks, in the ^{1}H NMR spectrum at the same temperature (179 K), one more similar set of singlets

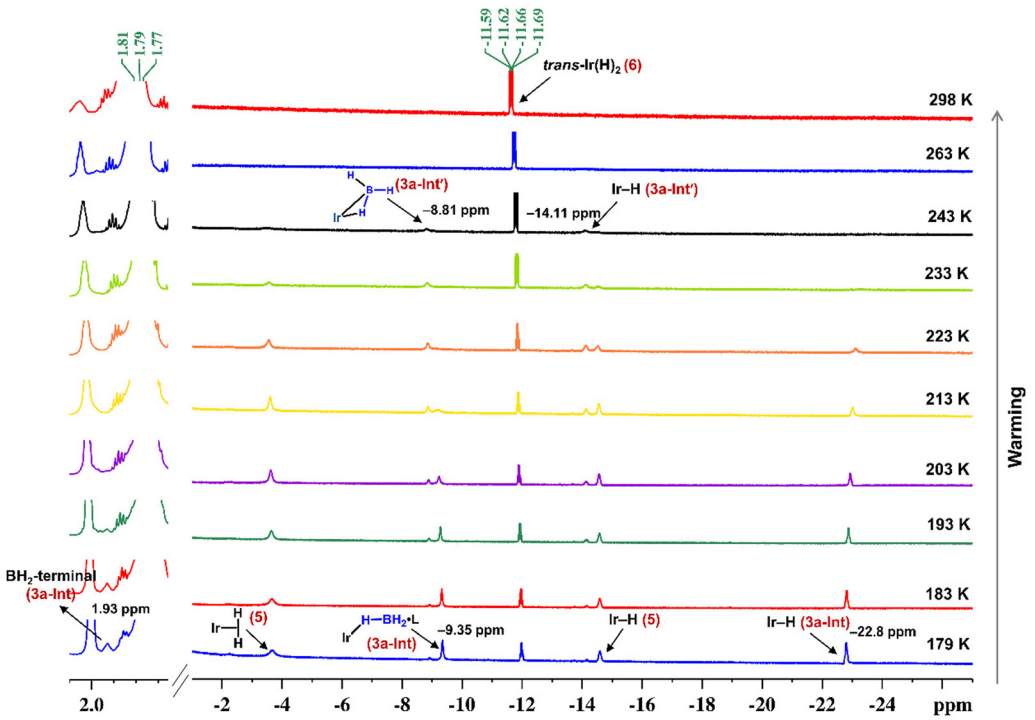

Fig. 5 Partial VT ^{1}H NMR (500.0 MHz, CD_2Cl_2) spectral stack plot of monitoring the reaction of [Ir(H)(PMe_3)(^{tBu4}POCOP)][BAr^F_4] (**3**) with H_3B·THF from 179 to 298 K (pre-cooled probe experiment).

at −8.81 and −14.11 ppm also appeared (Fig. 5). These peaks could be ascribed to the B–H bond of the bound H_3B and Ir–H, respectively, in another intermediate species, *trans*-[Ir(H)(η^2-HBH_2)PMe_3(^{tBu4}POCOP)][BAr^F_4] (**3a-Int′**; the structure was optimized computationally), wherein the B–H bond of BH_3 is in η^2-binding mode with the metal center. A similar binding mode of the B–H bond of BH_3 was observed in the reported σ-borane complex, [(^{tBu}POCOP)IrH_2(BH_3)].[18]

At this temperature, in the ^{1}H NMR spectrum, signals due to complex **6** were also noted, the concentration of which was low. Upon warming up the sample, we noted an increase in the signal intensity of intermediate **3a-Int′**. Upon warming up the sample, the peaks of both the intermediate species disappeared and resulted in the formation of complex **6**. In addition to the hydride peaks in the ^{1}H NMR spectra and the peaks for the pincer and the PMe_3 ligand in the $^{31}P\{^{1}H\}$ NMR spectra, the formation of intermediates, **3a-Int** and **3a-Int′**, was supported also by the peaks observed for the pincer ligands in these species in the ^{1}H NMR spectrum.

To gain insights into this reactivity, we carried out computational studies on this reaction. The computational studies revealed the mechanism of *trans*-[Ir(H)$_2$$PMe_3$(^{tBu4}POCOP)] (**6**) formation. Initially, the B–H bond of H_3B·THF coordinates to the sixth coordination site of complex **3**, forming intermediate **3a-Int** (Fig. 6 and 7) with a $\Delta G_{(sol)}$ of −4.8 kcal mol^{-1}. Subsequently, a THF molecule attacks the boron center of the coordinated borane in **3a-Int**, facilitating B–H bond cleavage. This process further generates the six-coordinate Ir(III) *trans*-dihydride complex **6** *via* a transition state (TS) with an energy barrier of +17.2 kcal mol^{-1} (Fig. 6 and 8). The heterolytic cleavage of the B–H bond in the coordinated H_3B·THF results in the transfer of hydride to the iridium center, forming complex **6** along with a boronium compound, [H_2B(THF)$_2$][BAr^F_4], as a byproduct. The formation of complex **6** was found to be exergonic by 0.3 kcal mol^{-1} ($\Delta G_{(sol)}$). The reaction from **3a-Int** to **6** is endergonic by 4.5 kcal mol^{-1}, which indicates that the reverse barrier (from **6** to **3a-int**) would be lower than the forward barrier (from **3a-int** to **6**). It should, however, be noted that the forward reaction involves the interaction of the less bulky THF molecule with **3a-int**, while the reverse reaction would involve the reaction between two bulky moieties: [H_2B(THF)$_2$][BAr^F_4] and **6**. It is noted that the counter anion, $BAr^F_4{}^-$, has not been included in the calculations due to computational expense, but its presence would further serve to increase the steric congestion that would be felt during the reverse reaction from **6** to **3a-int**. Hence, the reverse reaction would be less favoured than the forward reaction, and complex **6** would be the preferred product in the reaction.

Additionally, an optimized structure of **3a-Int′** could also be obtained without THF (Fig. 7). The optimized geometries of **3a-Int** and **3a-Int′** revealed distinct B–H bond distances to the metal center: 1.29 and 1.32 Å in **3a-Int** and **3a-Int′**, respectively (Fig. 7). This minimal difference in the bond distances is due to the different binding modes. In **3a-Int**, the B–H hydrogen is

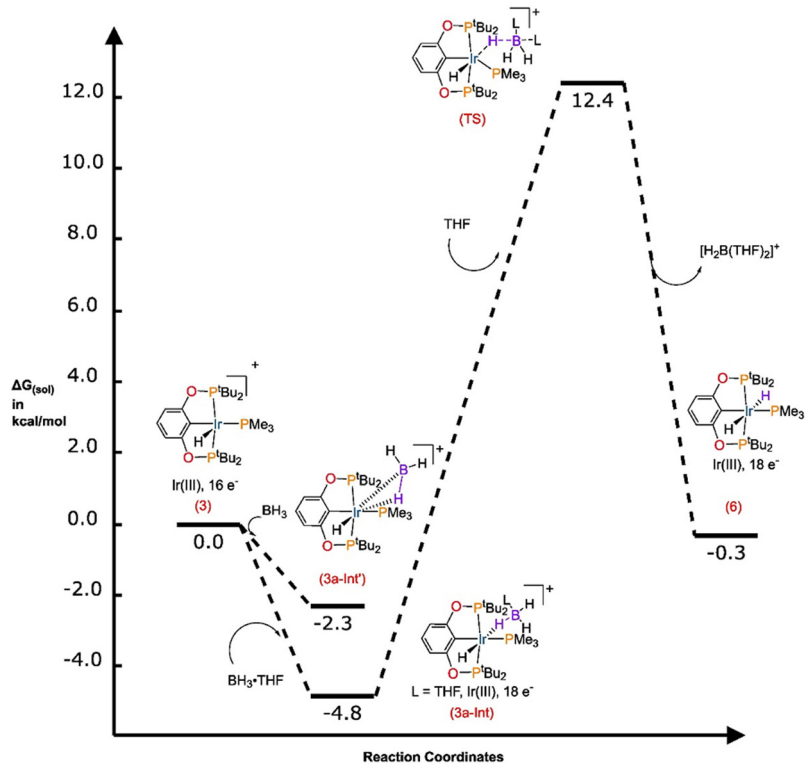

Fig. 6 Free energy profile of the reaction of complex **3** with $H_3B{\cdot}THF$.

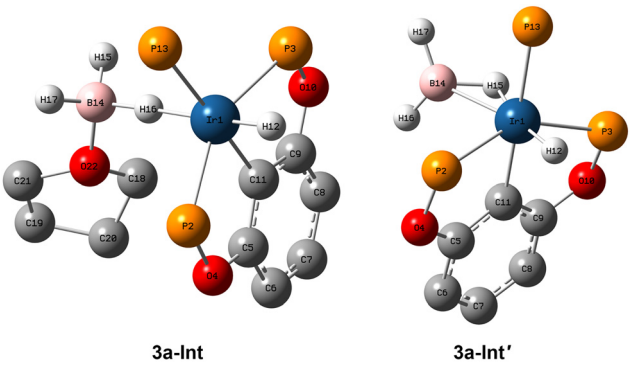

Fig. 7 Optimized geometries of complexes **3a-Int** and **3a-Int′**. Selected bond lengths in complex **3a-Int** (Å): Ir1–H16, 1.912; B14–H16, 1.287; Ir1–B14, 3.184; Ir1–H15, 3.819; Ir1–H17, 3.651; Ir1–H12, 1.566. Selected bond lengths in complex **3a-Int′** (Å): Ir1–H15, 1.70; B14–H15, 1.321; Ir1–B14, 2.263; Ir1–H16, 3.013; Ir1–H17, 3.078; Ir1–H12, 1.603. Atom color: C-grey, H-white, O-red, P-orange, and Ir-dark blue.

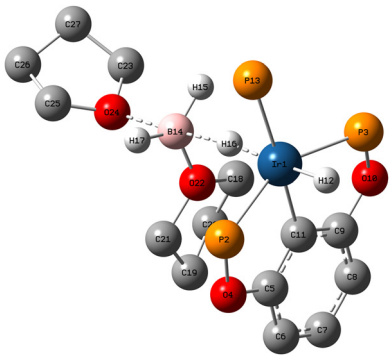

Fig. 8 Optimized geometry of the TS.

shared between two electrophilic centers (the cationic iridium and the Lewis acidic borane), resulting in a zwitterionic-type interaction. The more electrophilic borane center than the iridium in **3a-Int** pulls the H-atom closer to boron, resulting in a shorter B–H bond. Conversely, **3a-Int′** exhibits the η^2-binding mode wherein the B–H σ-bonding electrons are shared with the iridium center. This interaction weakens the B–H bond, accounting for its longer bond distance. Energetically, **3a-Int** ($\Delta G_{(sol)}$ is −4.8 kcal mol^{-1}) was found to be more stable than **3a-Int′** ($\Delta G_{(sol)}$ is −2.3 kcal mol^{-1}).

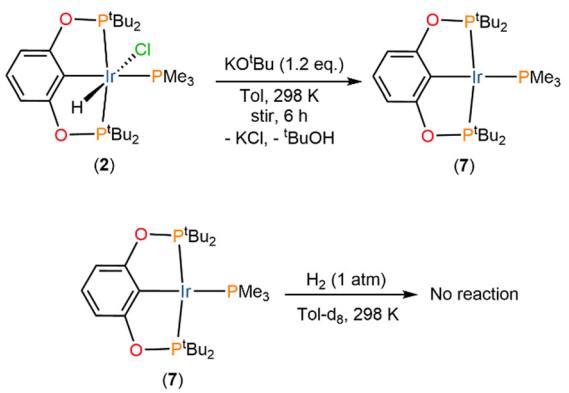

(3)

(4)

Additionally, the formation of complex **5** was also noted at 179 K. It indicates that H_2 is generated in the reaction mixture.

The presence of the boronium compound, $[BH_2(THF)_2][BAr^F_4]$, suggests that the likely pathway for H_2 generation is a side reaction involving reduction of the iridium center from Ir(III) to Ir(I) in complex **3** assisted by $H_3B{\cdot}THF$, resulting in the formation of a four-coordinate Ir(I) complex, $[Ir(PMe_3)(^{tBu4}POCOP)]$ (**7**), $[BH_2(THF)_2][BAr^F_4]$, and H_2. However, complex **7** could not be observed using NMR spectroscopy in the reaction of complex **3** to afford complex **6**. We anticipated that complex **7** would react instantaneously with H_2 to yield complex **6**. To test this hypothesis, in an independent reaction, complex **7** was prepared by reacting complex **2** with 1.2 equiv. of KO^{t}Bu (eqn (3)); the resulting complex **7** was allowed to react with H_2 (1 atm) at room temperature (eqn (4)). However, no reaction was apparent (Fig. S123 and S124). Within this reaction scheme, the pathway by which H_2 is generated could not be identified. Yet, as soon as H_2 evolves, it reacts with complex **3** to give complex **5**. In an independent reaction of complex **3** with H_2 (eqn (2)), the formation of complex **5** was only noted. This shows that complex **6** does not form from complex **5**. Additionally, as observed in the independent reaction previously (eqn (2), Fig. 3), the peaks of complex **5** disappeared as the sample was warmed up to 253 K, which is due to the rapid intermolecular exchange between the bound H_2 and the free H_2. This was evident from the appearance of a singlet at 4.6 ppm for free H_2 at 298 K (Fig. S66). At this temperature, the decoordination of the bound H_2 generates complex **3**, which instantaneously reacts with $H_3B{\cdot}THF$ to form complex **6**.

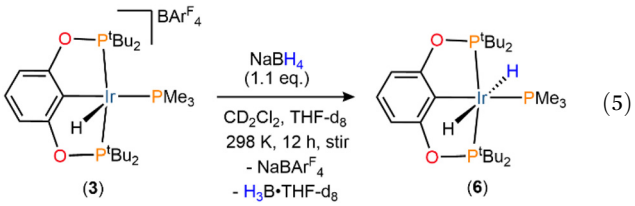

(5)

Formation of complex **6** in the reaction was authenticated by preparing it *via* the reaction of complex **3** with 1.1 equiv. of $NaBH_4$ in a solvent mixture of CD_2Cl_2 and THF-d_8 (1 : 1 volume ratio) (eqn (5)). This reaction afforded complex **6** *via* an activation of the B–H bond in the borohydride. Complex **6** was found to be unstable under vacuum. Therefore, it was isolated by evaporating the solvents under an Ar flow.

Reaction of the $[Ir(H)(PMe_3)(^{tBu4}POCOP)][BAr^F_4]$ complex (3) with $H_3B{\cdot}NMe_3$ and $H_3B{\cdot}NMe_2H$ (DMAB)

To gain further insights into the mechanism of B–H bond activation in neutral boranes ($H_3B{\cdot}L$; L = Lewis base), reactions of complex **3** with $H_3B{\cdot}NMe_3$ and $H_3B{\cdot}NMe_2H$ were investigated. Interestingly, no reaction was observed between complex **3** and $H_3B{\cdot}NMe_3$ at room temperature (Scheme 3). However, $H_3B{\cdot}NMe_2H$ reacted with complex **3** at 298 K (Scheme 3), resulting in the formation of complex **5** and cyclic diborazane, $[H_2BNMe_2]_2$, along with the presence of complex **3** in 30 min. At 298 K, after 30 min of the reaction, in the ^{1}H NMR spectrum, a broad signal at −42.21 ppm appeared (Fig. 9).

In order to obtain finer details of the broad spectral feature, the sample was cooled gradually up to 183 K and the NMR

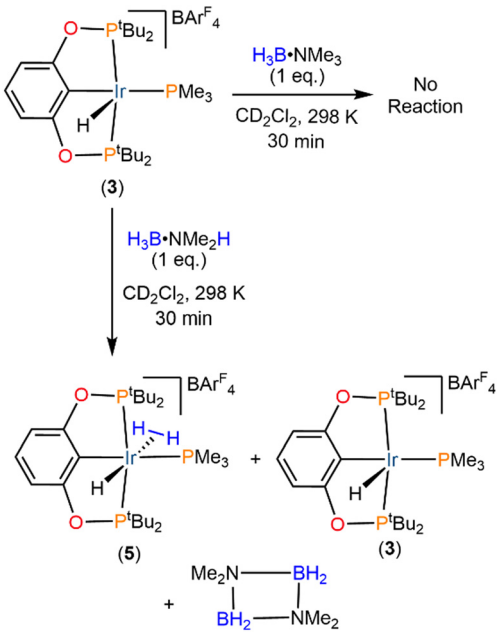

Scheme 3 Reaction of $[Ir(H)(PMe_3)(^{tBu4}POCOP)][BAr^F_4]$ (**3**) with $H_3B{\cdot}NMe_3$ and $H_3B{\cdot}NMe_2H$ at 298 K.

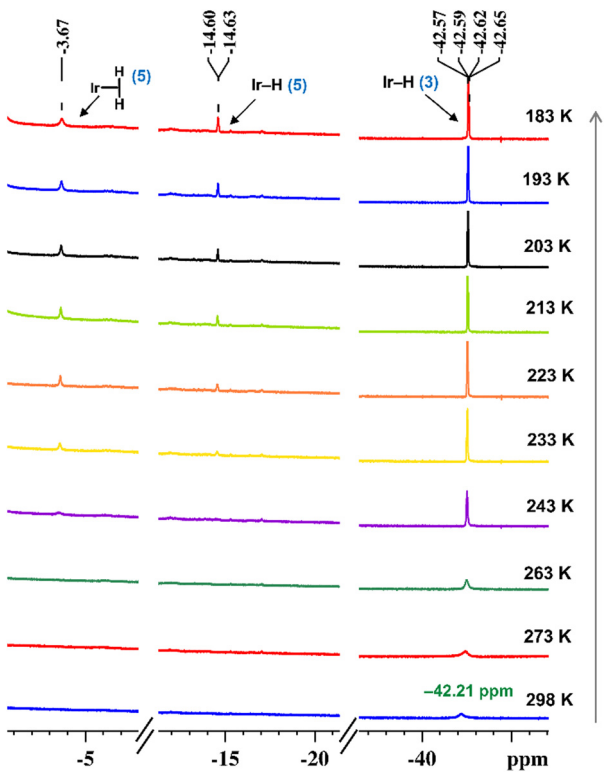

Fig. 9 Partial VT ^{1}H NMR (500.0 MHz, CD_2Cl_2) spectral stack plot of the reaction of $[Ir(H)(PMe_3)(^{tBu4}POCOP)][BAr^F_4]$ (**3**) with $H_3B{\cdot}NMe_2H$ after 30 min.

spectral data were acquired (Fig. 9). The broad signal sharpened upon lowering the temperature and resolved into a quartet at −42.61 ppm from 233 to 183 K, which was assigned

to complex **3**. Simultaneously, two broad singlets at −3.58 and −14.55 ppm started appearing from 233 K. The intensity of the singlets increased upon lowering the temperature, and they appeared as a singlet and quartet at −3.67 and −14.62 ppm at 183 K, respectively. The spectral pattern of complex **5** obtained herein matched with that of the product obtained in the separate reaction of complex **3** with H_2 (Fig. 3), indicating the formation of complex **5** along with $[H_2BNMe_2]_2$ *via* activation of the B–H bond in $H_3B{\cdot}NMe_2H$.

To investigate the mechanism, the reaction was monitored as a function of time. After 10 min of the reaction, a quartet at −11.65 ppm appeared in the ^{1}H NMR spectrum at 298 K (Fig. 10), which is ascribed to the dihydride complex (**6**) as noted in the reactions of complex **3** with $H_3B{\cdot}THF$ and $NaBH_4$ (Scheme 2 and eqn (5)). The intensity of the quartet for complex **6** was invariant with respect to temperature (Fig. 10), indicating that the appearance of the additional peaks upon lowering the temperature is not related to the quartet for complex **6**.

It was also confirmed by performing an independent VT NMR experiment of complex **6** alone, in which no change was observed in the hydride region (Fig. S82). Upon lowering the temperature, in the ^{1}H NMR spectrum, two broad signals appeared at −10.20 and −23.15 ppm at 213 K (Fig. 10). They resolved into a sharp singlet and a quartet, respectively, upon further cooling, suggesting the formation of a σ-borane complex, *trans*-[Ir(H)(η^1-$HBH_2{\cdot}NMe_2H$)PMe_3(^{tBu4}POCOP)][BAr^F_4] (**3b**) (Scheme 4, step 1). The singlet and quartet could be assigned to the bound B–H bond and Ir–H in the complex, respectively. Along with the hydride signals at −10.20 and −23.15 ppm, peaks were noted for the pincer ligand as well in the ^{1}H NMR spectrum, which supports the formation of complex **3b**. A ^{1}H–^{1}H COSY NMR spectrum showed a correlation between the signals at −10.20 and 1.33 ppm (for terminal B–H of the bound DMAB), confirming a σ-borane complex (Fig. S109).

The chemical shift values for the σ-borane complex matched with those of the reported complexes, [Ir(^{i}Pr-PN^{H}P)(H)$_2$(η^1-$H_3B{\cdot}NMe_3$)][BAr^F_4][14] and [Rh(κ^3-POP-Xantphos)(H)$_2$(η^1-$H_3B{\cdot}NMe_2H$)][BAr^F_4],[27] by Weller and co-workers. However, due to spectral broadening at low temperatures, the bound DMAB in complex **3b** was not characterized using the ^{11}B NMR spectrum (Fig. S112).

The formation of complex **6** and the boronium compound, $[(NHMe_2)_2BH_2][BAr^F_4]$ (**A**) (δ_A −2.3, br t, $^1J_{BH}$ = 115 Hz, Fig. 11), suggests that the next step involves heterolytic cleavage of the bound B–H bond in intermediate **3b** (Scheme 4, step 2). Subsequently, the next step involves protonation of the Ir–H bond in complex **6** by the acidic NH group of the boronium compound, $[(NHMe_2)_2BH_2][BAr^F_4]$ (**A**), resulting in the formation of complex **5** and the borazane monomer, $H_2B{=}NMe_2$ (**B**) (δ_B 37.4, br t, $^1J_{BH}$ = 126 Hz) (Scheme 4, step 3). The borazane monomer further undergoes cyclization to form the cyclic diborazane, $[H_2BNMe_2]_2$ (**C**), (δ_C 5.1, br t, $^1J_{BH}$ = 114 Hz).

Conejero and co-workers reported a similar reaction of the $[Pt(I^tBu')(I^tBu)]^+$ complex (I^tBu = 1,3-di-*tert*-butylimidazol-2-

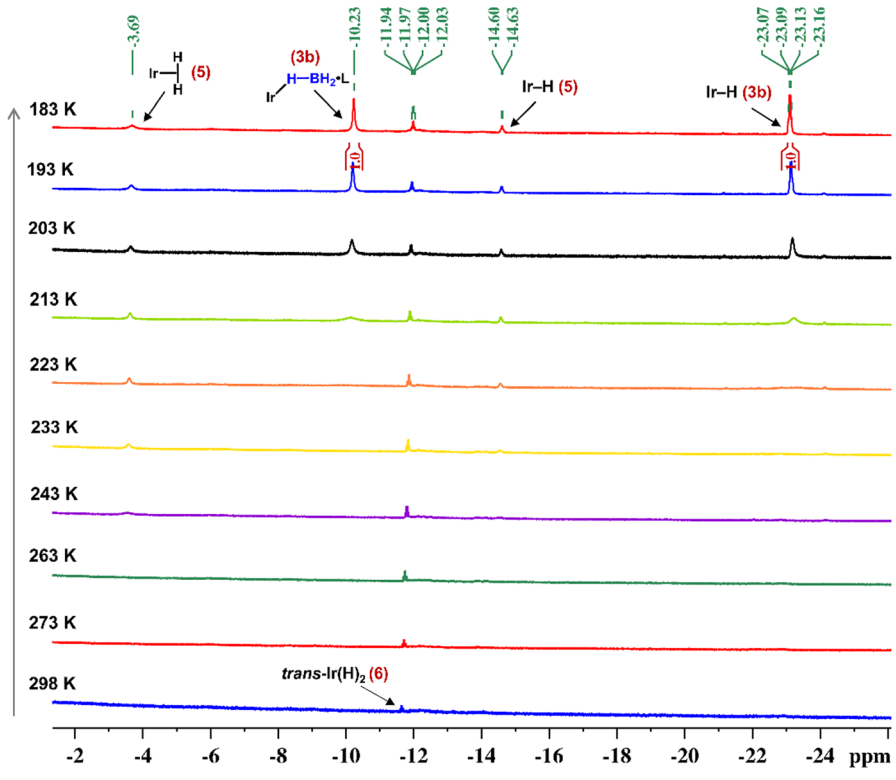

Fig. 10 Partial VT ^{1}H NMR (500.0 MHz, CD_2Cl_2) spectral stack plot of the reaction of [Ir(H)(PMe_3)(^{tBu4}POCOP)][BAr^F_4] (**3**) with $H_3B{\cdot}NMe_2H$ after 10 min.

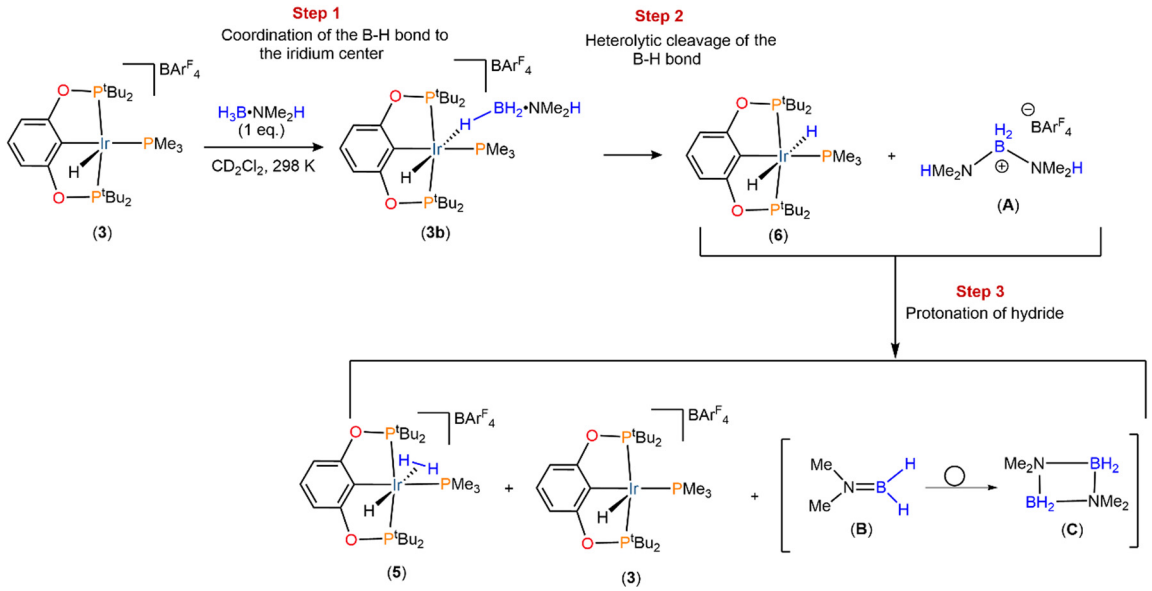

Scheme 4 Monitoring of the reaction of [Ir(H)(PMe$_3$)(^{tBu4}POCOP)][BAr$^F_4$] (**3**) with H$_3$B·NMe$_2$H at 298 K.

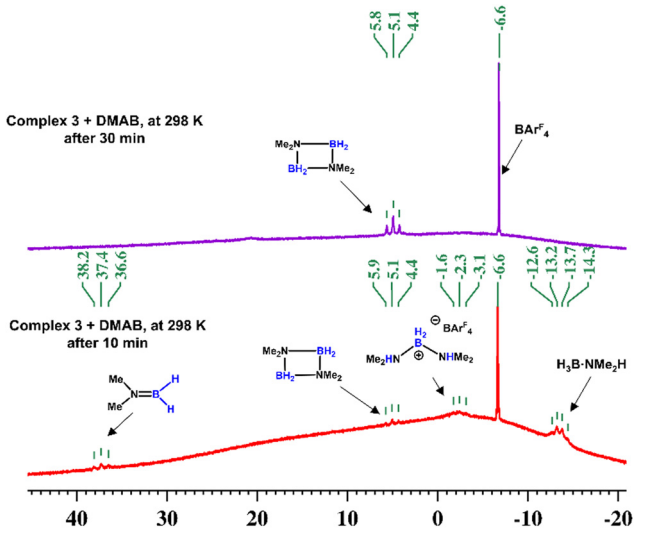

Fig. 11 Partial ^{11}B NMR (160.4 MHz, CD_2Cl_2) spectral stack plot of monitoring the reaction of [Ir(H)(PMe$_3$)(^{tBu4}POCOP)][BAr$^F_4$] (**3**) with H$_3$B·NMe$_2$H.

ylidene, I^{t}Bu′ = cyclometalated I^{t}Bu ligand) with H$_3$B·NMe$_2$H.[48,49] In this case also, boron compounds **A**, **B**, and **C** (Fig. 11) with similar reaction steps have been observed. Similar to the NMR spectral pattern of complex **5**, the peaks of complex **3b** were also observed only at low temperatures due to an exchange of DMAB involving binding and lability as a result of a weak binding of the B–H σ-bond to the iridium center at 298 K. The rate of exchange slowed down at low temperatures. Thereafter, the solution was warmed to 298 K, and after an additional 10 min, the observed NMR spectral pattern at 298 K and at low temperatures were similar to that of the initial reaction (Fig. 9) carried out at 298 K for 30 min.

The reactions of complex **3** with H$_3$B·L (L = THF, NMe$_3$, NHMe$_2$) indicate that B–H bond heterolytic cleavage highly depends on the Lewis base (L). The B–H bond cleavage takes place with H$_3$B·THF even at low temperatures. In contrast, H$_3$B·NMe$_2$H required ∼20 min for complete B–H bond cleavage at 298 K itself, while no reaction was observed with H$_3$B·NMe$_3$. These findings establish a clear reactivity order in the case of B–H bond activation: H$_3$B·THF > H$_3$B·NMe$_2$H > H$_3$B·NMe$_3$. In H$_3$B·THF, the boron center is more electron-deficient since THF is a weak Lewis base, leading to the facile B–H bond activation. Conversely, in H$_3$B·NMe$_3$, NMe$_3$, a strong Lewis base, electronically stabilizes the boron center, making it unreactive at 298 K.[50] Additionally, the three methyl groups possibly create a steric effect with the *tert*-butyl groups, hindering the approach of H$_3$B·NMe$_3$ to the iridium center.

Conclusions

Six- and five-coordinate complexes, [Ir(H)Cl(PMe$_3$)(^{tBu4}POCOP)] (**2**) and [Ir(H)(PMe$_3$)(^{tBu4}POCOP)][BAr$^F_4$] (**3**), have been prepared and characterized. The reaction of complex **3** with H$_2$ resulted in the formation of the *trans* σ-H$_2$ complex, *trans*-[Ir(H)(η^2-H$_2$)(PMe$_3$)(^{tBu4}POCOP)][BAr$^F_4$] (**5**), observed over the temperature range of 253 to 183 K. Moreover, the intact nature of the bound H$_2$ in complex **5** was unequivocally established by $T_{1,min}$, $^1J_{H,D}$, and d_{H-H} measurements. Furthermore, complex **3** brings about heterolytic cleavage of the B–H bond in H$_3$B·THF and H$_3$B·NMe$_2$H *via* the intermediate σ-borane complexes, *trans*-[Ir(H)(η^1-HBH$_2$·THF)PMe$_3$(^{tBu4}POCOP)][BAr$^F_4$] (**3a-Int**) and *trans*-[Ir(H)(η^1-HBH$_2$·NMe$_2$H)PMe$_3$(^{tBu4}POCOP)][BAr$^F_4$] (**3b**), respectively. The structural assignment of complex **3a-Int** was also supported by DFT calculations. Since the binding of H$_2$, H$_3$B·THF, and H$_3$B·NMe$_2$H to the iridium center in complex **3**

is weak at 298 K, the NMR spectral peaks of the corresponding σ-complexes were observed only at low temperatures. In the case of $H_3B{\cdot}NMe_2H$, the intermediate boron compounds, $[(NHMe_2)_2BH_2][BAr^F_4]$ (**A**) and $H_2B{=}NMe_2$ (**B**), could be characterized. In contrast, no reaction between complex **3** and $H_3B{\cdot}NMe_3$ was apparent. In summary, the reactivity of $H_3B{\cdot}L$ (L = THF, NMe_2H, NMe_3) with complex **3** was found to be in the order, $H_3B{\cdot}THF > H_3B{\cdot}NMe_2H > H_3B{\cdot}NMe_3$.

Experimental section

General procedures

Unless otherwise stated, all the reactions were carried out under a dry and oxygen-free N_2 or an Ar atmosphere using standard Schlenk or glovebox techniques. All the glassware was dried at 403 K for 12 h prior to use. Toluene was dried by refluxing over Na–benzophenone and distilled. CH_2Cl_2 and pentane were dried by refluxing over CaH_2 and distilled. CD_2Cl_2 and THF-d_8 were purchased from Cambridge Isotope Laboratories and dried over 4 Å and 5 Å molecular sieves, respectively. All the solvents were degassed thoroughly by freeze–pump–thaw before use. $H_3B{\cdot}NMe_2H$ and $H_3B{\cdot}NMe_3$ were purchased from Sigma-Aldrich and purified by sublimation prior to use.[51] $H_3B{\cdot}THF$ solution was also purchased from Sigma-Aldrich and purified by the trap-to-trap technique.[52] $[IrCl(COE)_2]_2$ (COE = *cis*-cyclooctene), (^{tBu4}POCOP), and [Ir(H)Cl(^{tBu4}POCOP)] (**1**) were prepared according to literature procedures.[53,54] Detailed experimental data are provided in the SI.

NMR spectra were recorded using Bruker Avance AV-500 500 MHz and AV-400 400 MHz spectrometers. The ^{1}H and ^{13}C $\{^1H\}$ NMR chemical shift values were referenced to the residual non-deuterated solvent signals of the corresponding deuterated solvents. ^{31}P and ^{11}B NMR chemical shift values were referenced to external standards, 85% H_3PO_3 and $H_3N{\cdot}BH_3$, respectively. ^{19}F NMR chemical shift values were referenced to $BF_3{\cdot}Et_2O$. Variable temperature ^{1}H spin–lattice relaxation time (T_1) measurements were performed using the standard inversion recovery method with the pulse sequence of 180°–τ–90° at 500 MHz. Mass spectra and elemental analyses were recorded using a Micromass Q-TOF (HRMS) spectrometer and a Thermo Scientific Flash 2000 Organic Elemental Analyzer, respectively.

Synthesis of [Ir(H)Cl(PMe$_3$)(^{tBu4}POCOP)] (2)

A toluene-d_8 (0.7 mL) solution of complex **1** (10.0 mg, 0.016 mmol) was prepared in an NMR tube. To this solution, PMe_3 (16.0 μL, 1.2 mg, 0.016 mmol; 1.0 M solution in toluene) was added. Immediately upon addition, the solution color turned from brown-red to light yellow. The formation of complex **2** was confirmed by ^{1}H and $^{31}P\{^1H\}$ NMR spectroscopy, and the NMR yield was calculated to be 91.4% using 1,4-dinitrobenzene as an internal standard. ^{1}H NMR (400.0 MHz, Tol-d_8, 298 K): δ 6.82 (t, $^3J_{H,H}$ = 7.9 Hz, 1H, 4-H), 6.64 (d, $^3J_{H,H}$ = 7.9 Hz, 2H, 3- and 5-H), 1.51 (d, $^2J_{H,P}$ = 8.2 Hz, PMe_3), 1.49 (pseudo triplet, $^3J_{H,P}$ = 6.7 Hz, ^{t}Bu), 1.08 (pseudo triplet, $^3J_{H,P}$ = 6.7 Hz, 18H, ^{t}Bu), −22.32 (td, $^2J_{H,Pin}$ = 14.4 Hz, $^2J_{H,PMe3}$ = 11.6 Hz, 1H, Ir–H). Since the peaks at 1.51 and 1.49 were overlapped, the integral value was calculated by considering both the peaks. It was found to be for 27 protons (27H; 9H for PMe_3 and 18H for ^{t}Bu). $^{31}P\{^1H\}$ NMR (161.9, Tol-d_8, 298 K): δ 157.6 (m, P(^{t}Bu)$_4$), −57.5 (m, PMe_3). $^{13}C\{^1H\}$ NMR (125 MHz, Tol-d_8, 298 K): δ 164.1 (t, $J_{C,P}$ = 5.2 Hz, Ar), 107.4 (s, Ar), 104.2 (t, $J_{C,P}$ = 5.8 Hz, Ar), 45.9 (t, $J_{C,P}$ = 11.4 Hz, Cq, ^{t}Bu), 41.2 (t, $J_{C,P}$ = 12.2 Hz, Cq, ^{t}Bu), 30.1 (vt, $J_{C,P}$ = 2.2 Hz, CH_3, ^{t}Bu), 29.4 (vt, $J_{C,P}$ = 2.6 Hz, CH_3, ^{t}Bu), 23.4 (d, $J_{C,P}$ = 30.0 Hz, PMe_3). HRMS (TOF, ESI, positive ion; *m*/*z*): calcd for $[M]^+$: 702.23, found: 702.2619. Complex **2** was isolated by slow evaporation of the solvent under an Ar flow. The isolated solid was redissolved in toluene-d_8. NMR spectroscopy evidenced the presence of both complexes **2** and **1**. The formation of complex **1** (minor) is due to the elimination of PMe_3 under the flow of Ar gas.

Synthesis of [Ir(H)(PMe$_3$)(^{tBu4}POCOP)][BAr$^F_4$] (3)

In a Schlenk tube, complex **2** was prepared in toluene (5 mL) from complex **1** (50 mg, 0.08 mmol) and PMe_3 (80.0 μL, 6.0 mg, 0.08 mmol; 1.0 M solution in toluene). To the solution of complex **2**, $NaBAr^F_4$ (85.0 mg, 0.096 mmol) was added. The reaction mixture was stirred at 273 K for 1 h. An orange-colored solid precipitated out during the reaction. The supernatant was decanted and the solid was washed with cold toluene (2 × 5 mL) and *n*-pentane (3 × 5 mL) using a filter frit. The solid was extracted with CH_2Cl_2 and the solvent was removed under vacuum. Complex **3** was isolated as an orange-colored solid in 90% (101.0 mg) yield. ^{1}H NMR (500.0 MHz, CD_2Cl_2, 298 K): δ 7.17 (t, $^3J_{H,H}$ = 8.0 Hz, 1H, 4-H), 6.82 (d, $^3J_{H,H}$ = 8.0 Hz, 2H, 3- and 5-H), 2.06 (d, $^2J_{H,P}$ = 8.3 Hz, 9H, PMe_3), 1.32 (pseudo triplet, ^{t}Bu), 1.27 (pseudo triplet, ^{t}Bu), −42.46 (dt, $^2J_{H,PMe3}$ = 20.0 Hz, $^2J_{H,Pin}$ = 10.0 Hz, 1H, Ir–H). The peaks at 1.32 and 1.27 ppm could not be integrated accurately due to signal broadening caused by the presence of grease. $^{31}P\{^1H\}$ NMR (161.9 MHz, CD_2Cl_2, 298 K): δ 180.5 (m, P(^{t}Bu)$_4$), −38.5 (m, PMe_3). ^{11}B NMR (128.3 MHz, CD_2Cl_2, 298 K): δ −6.6. $^{19}F\{^1H\}$ NMR (376.5 MHz, CD_2Cl_2, 298 K): δ −62.8. $^{13}C\{^1H\}$ NMR (100.6 MHz, CD_2Cl_2, 298 K): δ 166.9 (t, $J_{C,P}$ = 5.0 Hz, Ar), 132.0 (s, Ar), 105.6 (t, $J_{C,P}$ = 5.8 Hz, Ar), 45.4 (t, $J_{C,P}$ = 11.7 Hz, Cq, ^{t}Bu), 41.4 (t, $J_{C,P}$ = 13.5 Hz, Cq, ^{t}Bu), 29.0 (vt, $J_{C,P}$ = 2.8 Hz, CH_3, ^{t}Bu), 28.1 (vt, $J_{C,P}$ = 2.4 Hz, CH_3, ^{t}Bu), 26.1 (d, $J_{C,P}$ = 33.7 Hz, PMe_3). HRMS (TOF, ESI, positive ion; *m*/*z*): calcd for $[M]^+$: 667.2569, found: 667.2597.

Synthesis of [Ir(H)(THF)(PMe$_3$)(^{tBu4}POCOP)][BAr$^F_4$] (4)

The formation of complex **4** was monitored using NMR spectroscopy. To a Schlenk tube containing complex **3** (15 mg, 0.01 mmol), 0.5 mL of THF-d_8 was added. Upon addition of THF-d_8, the solution color immediately changed from orange to brown. The formation of complex **4** was confirmed by ^{1}H and $^{31}P\{^1H\}$ NMR spectroscopy. However, complex **4** was found to be unstable in solution and gradually converted into the [Ir(H)(THF)(^{tBu4}POCOP)][BAr$^F_4$] (**4a**) complex.

NMR data for complex 4. ^{1}H NMR (400.0 MHz, THF-d_8, 298 K): δ 6.71 (br, 1H, 4-H), 6.41 (br, 2H, 3- and 5-H), 2.81 (br, coordinated THF), 1.83 (d, $^2J_{H,P}$ = 8.2 Hz, 9H, PMe_3), 1.50 (pseudo triplet, $^3J_{H,P}$ = 6.9 Hz, 18H, ^{t}Bu), 1.29 (br, coordinated

THF), 1.26 (pseudo triplet, $^{3}J_{H,P}$ = 6.7 Hz, ^{t}Bu), −22.38 (br, 1H, Ir–H). Since the peaks at 1.29 and 1.26 were overlapped, the integral value for the peak at 1.26 ppm could not be determined accurately. $^{31}P\{^{1}H\}$ NMR (161.9, THF-d_8, 298 K): δ 158.0 (br, $P(^{t}Bu)_4$), −57.3 (br, PMe_3).

NMR data for complex 4a. ^{1}H NMR (400.0 MHz, THF-d_8, 298 K): δ 6.71 (t, $^{3}J_{H,H}$ = 8.0 Hz, 4-H), 6.49 (d, $^{3}J_{H,H}$ = 8.0 Hz, 2H, 3- and 5-H), 1.35 (pseudo quartet, 36H, ^{t}Bu), −40.94 (t, $^{2}J_{H,P}$ = 12.0 Hz, 1H, Ir–H). $^{31}P\{^{1}H\}$ NMR (161.9, THF-d_8, 298 K): δ 174.9 (s, $P(^{t}Bu)_4$).

Reaction of complex 3 with H_2 to form the *trans*-[Ir(H)(η^2-H_2)(PMe_3)(^{tBu4}POCOP)][BAr^{F}_4] complex (5)

To a 0.5 mL CD_2Cl_2 solution of complex **3** (15 mg, 0.01 mmol), H_2 at 1 bar pressure was introduced in a pressure-stable NMR tube. The tube was then agitated on an NMR tube shaker for 10 min to ensure thorough mixing. The reaction progress was monitored using variable-temperature (VT) NMR spectroscopy, with the temperature gradually lowered from 298 to 178 K. At 253 K, the formation of the *trans*-[Ir(H)(η^2-H_2)(PMe_3)(^{tBu4}POCOP)][BAr^{F}_4] complex (**5**) was observed. As the temperature was further lowered to 178 K, the signal intensity corresponding to complex **5** increased significantly. At 213 K, ^{1}H, $^{31}P\{^{1}H\}$ and $^{13}C\{^{1}H\}$ NMR spectra were acquired for complex **5**. ^{1}H NMR (500.0 MHz, CD_2Cl_2, 213 K): δ 6.92 (t, $^{3}J_{H,H}$ = 7.9 Hz, 1H, 4-H), 6.57 (d, $^{3}J_{H,H}$ = 7.9 Hz, 2H, 3- and 5-H), 1.83 (d, $^{2}J_{H,P}$ = 8.8 Hz, 9H, PMe_3), 1.34 (pseudo triplet, ^{t}Bu), 1.22 (pseudo triplet, ^{t}Bu), −3.63 (br s, 2H, Ir(η^2-H_2)), −14.57 (q, $^{2}J_{H,P}$ = 14.0 Hz, 1H, Ir–H). The peaks at 1.34 and 1.22 ppm could not be integrated accurately due to signal broadening caused by the presence of grease. $^{31}P\{^{1}H\}$ NMR (202.4 MHz, CD_2Cl_2, 213 K): δ 172.0 (br s, $P(^{t}Bu)_4$), −64.9 (br s, PMe_3). $^{13}C\{^{1}H\}$ NMR (125.7 MHz, CD_2Cl_2, 213 K): δ 162.2 (s, Ar), 128.0 (s, Ar), 104.8 (vt, $J_{C,P}$ = 5.8 Hz, Ar), 42.8 (t, $J_{C,P}$ = 13.0 Hz, Cq, ^{t}Bu), 38.0 (t, $J_{C,P}$ = 12.7 Hz, Cq, ^{t}Bu), 28.4 (s, CH_3, ^{t}Bu), 27.2 (s, CH_3, ^{t}Bu), 25.4 (d, $J_{C,P}$ = 35.2 Hz, PMe_3).

Reaction of complex 3 with H_3B·THF to form the *trans*-[Ir($H)_2$(PMe_3)(^{tBu4}POCOP)] complex (6), [$H_2B(THF)_2$][BAr^{F}_4] and H_2 at 298 K

To the CD_2Cl_2 (0.5 mL) solution of complex **3** (20.0 mg, 0.013 mmol), H_3B·THF (15.6 μL, 1.3 mg, 0.0156 mmol; 1.0 M solution in THF) was added at 298 K in a Young's NMR tube. Immediately, the color of the solution changed from orange to pale yellow. During the reaction, H_2 gas evolved. The formation of complex **6**, the [$H_2B(THF)_2$][BAr^{F}_4] adduct and H_2 was established using NMR spectroscopy. Complex **6** could not be isolated as it is not stable in the reaction mixture.

NMR data for the *trans*-[Ir($H)_2$(PMe_3)(^{tBu4}POCOP)] complex (6). ^{1}H NMR (500.0 MHz, CD_2Cl_2, 298 K): δ 6.62 (t, $^{3}J_{H,H}$ = 7.8 Hz, 1H, 4-H), 6.30 (d, $^{3}J_{H,H}$ = 7.8 Hz, 2H, 3- and 5-H), 1.78 (d, $^{2}J_{H,P}$ = 8.0 Hz, PMe_3), 1.36 (pseudo triplet, 36H, ^{t}Bu), −11.63 (q, $^{2}J_{H,P(cis)}$ = 15.0 Hz, 2H, Ir–H). The signal at 1.78 ppm for the PMe_3 ligand could not be integrated as it is overlapping with the THF solvent signal. $^{31}P\{^{1}H\}$ NMR (161.9 MHz, CD_2Cl_2, 298 K): δ 176.2 (d, $^{2}J_{P,PMe3}$ = 8.0 Hz, $P(^{t}Bu)_4$), −68.6 (t, $^{2}J_{PMe3,P}$ = 8.0 Hz, PMe_3).

NMR data for [$H_2B(THF)_2$][BAr^{F}_4]. $^{1}H\{^{11}B\}$ NMR (500.0 MHz, CD_2Cl_2, 298 K): δ 2.89 (br s, BH_2). ^{11}B NMR (128.3 MHz, CD_2Cl_2, 298 K): δ 9.3 (br t, $^{1}J_{B,H}$ = 130.5 Hz). $^{11}B\{^{1}H\}$ NMR (160.4 MHz, CD_2Cl_2, 298 K): δ 9.3 (s).

Reaction of complex 3 with H_3B·THF at 179 K

A 0.4 mL CD_2Cl_2 solution of complex **3** (20.0 mg, 0.013 mmol) was taken in a Schlenk NMR tube. It was then immersed in a liquid nitrogen bath and 0.2 mL of CD_2Cl_2 solution of BH_3·THF (15.6 μL, 1.3 mg, 0.0156 mmol; 1.0 M solution in THF) was added along the walls of the NMR tube under a positive flow of Ar gas. The stopcock was quickly replaced and the tube was evacuated for 30 min. Then the stopcock was closed tightly, and the tube was flame sealed in the frozen state. It was then inserted into the NMR probe, which was precooled to 179 K. The progress of the reaction was monitored by acquiring the ^{1}H, $^{1}H\{^{11}B\}$ $^{31}P\{^{1}H\}$, ^{11}B, and $^{11}B\{^{1}H\}$ spectra of the sample as the temperature was raised. The reaction was monitored from 179 to 298 K. Formation of complexes, *trans*-[Ir(H)(η^2-H_2)(PMe_3)(^{tBu4}POCOP)][BAr^{F}_4] (**5**), *trans*-[Ir($H)_2$(PMe_3)(^{tBu4}POCOP)] (**6**), *trans*-[Ir(H)(η^1-HBH_2·THF) PMe_3(^{tBu4}POCOP)][BAr^{F}_4] (**3a-Int**), and *trans*-[Ir(H)(η^2-HBH_2) PMe_3(^{tBu4}POCOP)][BAr^{F}_4] (**3b-Int′**) were observed.

NMR data for *trans*-[Ir(H)(η^1-HBH_2·THF) PMe_3(^{tBu4}POCOP)][BAr^{F}_4] (3a-Int). ^{1}H NMR (500.0 MHz, CD_2Cl_2, 179 K): δ 6.82 (t, 1H, 4-H), 6.45 (d, 2H, 3- and 5-H), 1.93 (s, 2H, BH_2 (terminal)) −9.35 (br s, 1H, Ir(η^1-HBH_2·THF)), −22.8 (q, $^{2}J_{H,P}$ = 16.0 Hz, 1H, Ir–H). Assignment of the PMe_3 and ^{t}Bu proton signals was not possible, as they appear broad at this temperature. $^{31}P\{^{1}H\}$ NMR (202.4 MHz, CD_2Cl_2, 179 K): δ 169.5 (br s, $P(^{t}Bu)_4$), −56.7 (br s, PMe_3). In the ^{11}B NMR spectrum, the peak of the bound H_3B·THF in complex **3a-Int** was not observed due to spectral broadening at low temperatures.

NMR data for complex 3a-Int′. ^{1}H NMR (500.0 MHz, CD_2Cl_2, 213 K): δ −8.81 (br s), −14.11 (Ir–H). $^{31}P\{^{1}H\}$ NMR (202.4 MHz, CD_2Cl_2, 213 K): δ 174.5 (br s, $P(^{t}Bu)_4$), −57.8 (br s, PMe_3).

NMR data for [$H_2B(THF)_2$][BAr^{F}_4]. $^{1}H\{^{11}B\}$ NMR (500.0 MHz, CD_2Cl_2, 179–298 K): δ 2.89 (br s, BH_2) (the signal intensity increased with increasing temperature).

Synthesis of [Ir(PMe_3)(^{tBu4}POCOP)] (7)

In a Schlenk tube, to a toluene (5 mL) solution of complex **1** (50.0 mg, 0.08 mmol), PMe_3 (80.0 μL, 6.0 mg, 0.08 mmol; 1.0 M solution in toluene) was added. Upon addition, the color of the solution changed from brown-red to light yellow immediately, indicating the formation of complex **2**, as confirmed by ^{1}H and $^{31}P\{^{1}H\}$ NMR spectroscopy. Subsequently, KO^{t}Bu (10.8 mg, 0.096 mmol) was added, and the reaction mixture was stirred at 298 K for 6 h. During the reaction, the solution color further changed from light yellow to orange. The solvent was removed under vacuum and the solid was washed with cold *n*-pentane (3 × 5 mL) and filtered using a filter frit. The solid was extracted with toluene, followed by solvent removal under vacuum. Finally, the solid was heated at 55 °C under vacuum to remove the toluene completely, affording complex **7**

as a yellow colored solid (43.1 mg, 81%). ^{1}H NMR (400.0 MHz, Tol-d_8, 298 K): δ 6.99 (4-H), 6.79 (d, $^{3}J_{H,H}$ = 7.8 Hz, 2H, 3- and 5-H), 1.56 (d, $^{2}J_{H,P}$ = 8.0 Hz, PMe_3), 1.30 (pseudo triplet, $^{3}J_{H,P}$ = 6.6 Hz, 36H, ^{t}Bu). The multiplicity and integration of the peak at 6.99 ppm were not determined due to its overlap with the aryl protons of the residual solvent in toluene-d_8. ^{31}P{^{1}H} NMR (161.9, Tol-d_8, 298 K): δ 187.0 (d, $^{2}J_{P,P}$ = 5.3 Hz, P(^{t}Bu)$_4$), −38.9 (t, $^{2}J_{P,P}$ = 5.3 Hz, PMe_3). ^{13}C{^{1}H} NMR (100.6 MHz, Tol-d_8, 298 K): δ 166.8 (s, Ar), 102.9 (vt, $J_{C,P}$ = 6.0 Hz, Ar), 41.8 (t, $J_{C,P}$ = 11.5 Hz, Cq, ^{t}Bu), 29.7 (t, $J_{C,P}$ = 3.5 Hz CH_3, ^{t}Bu), 28.3 (dt, $J_{C,P}$ = 27.5 Hz, $J_{C,P}$ = 2.1 Hz, PMe_3). HRMS (TOF, ESI, positive ion; *m*/*z*): calcd for [M]$^{+}$: 666.2491, found: 666.2509. Elemental analysis for $C_{25}H_{48}IrO_2P_3$: calcd: C, 45.10; H, 7.27; found: C, 45.53; H, 7.76.

Synthesis of *trans*-[Ir(H)$_2$(PMe$_3$)(^{t}Bu^{4}POCOP)] (6) from the reaction of complex 3 with NaBH$_4$

$NaBH_4$ (0.6 mg, 0.016 mmol) was added to a 0.3 mL CD_2Cl_2 solution of complex **3** (20.0 mg, 0.013 mmol) in a Schlenk tube. Then 0.3 mL of THF-d_8 was added to it. The reaction mixture was stirred for 12 h at 298 K. The orange solution turned pale yellow during the reaction. Complex **6** decomposed under vacuum. Therefore, the solvent was removed under an Ar gas flow. Then the residue was washed with *n*-pentane at 179 K and dried under an Ar gas flow to afford complex **6**. ^{1}H NMR (500.0 MHz, CD_2Cl_2 + THF-d_8, 298 K): δ 6.55 (t, $^{3}J_{H,H}$ = 7.8 Hz, 1H, 4-H), 6.25 (d, $^{3}J_{H,H}$ = 7.8 Hz, 2H, 3- and 5-H), 1.75 (d, $^{2}J_{H,P}$ = 8.0 Hz, PMe_3), 1.32 (pseudo triplet, 36H, ^{t}Bu), −11.64 (q, $^{2}J_{H,P(cis)}$ = 15.0 Hz, 2H, Ir–H). The signal at 1.75 ppm for the PMe_3 ligand could not be integrated as it is overlapping with the THF signal. ^{31}P{^{1}H} NMR (202.4 MHz, CD_2Cl_2, 298 K): δ 176.1 (d, $^{2}J_{P,PMe3}$ = 8.0 Hz, P(^{t}Bu)$_4$), −68.6 (t, $^{2}J_{PMe3,P}$ = 8.0 Hz, PMe_3). ^{13}C{^{1}H} NMR (125.7 MHz, CD_2Cl_2, 298 K): δ 162.7 (s, Ar), 122.8 (s, Ar), 102.7 (vt, $J_{C,P}$ = 5.8 Hz, Ar), 40.5 (t, $J_{C,P}$ = 12.8 Hz, Cq, ^{t}Bu), 29.3 (t, $J_{C,P}$ = 2.9 Hz CH_3, ^{t}Bu), 25.4 (d, PMe_3, half of the doublet is overlapping with the THF signal). HRMS (TOF, ESI, positive ion; *m*/*z*): calcd for [M]$^{+}$: 668.2647, found: 668.2640. Elemental analysis for $C_{25}H_{50}IrO_2P_3$: calcd: C, 44.96; H, 7.55; found: C, 45.37; H, 8.05.

Reaction of complex 3 with DMAB at 298 K

DMAB (0.8 mg, 0.014 mmol) was taken in a vial and a CD_2Cl_2 (0.5 mL) solution of complex **3** (20.0 mg, 0.013 mmol) was added to it at 298 K. Immediately the color of the solution changed from orange to yellow. Then the reaction mixture was transferred to a Young's NMR tube and NMR spectral data were acquired after 10 min. At 298 K, since the NMR spectral pattern was broad, a VT NMR study was carried out in order to assign all the species. Formation of *trans*-[Ir(H)$_2$(PMe$_3$)(^{t}Bu^{4}POCOP)] (**6**) was observed at 298 K, whereas *trans*-[Ir(H)(η^{2}-H$_2$)(PMe$_3$)(^{t}Bu^{4}POCOP)][BAr$^{F}_4$] (**5**) and *trans*-[Ir(H)(η^{1}-HBH$_2$·NMe$_2$H)PMe$_3$(^{t}Bu^{4}POCOP)][BAr$^{F}_4$] complexes (**3b**) were characterized at low temperatures. Formation of boron compounds such as [(NHMe$_2$)$_2$BH$_2$][BAr$^{F}_4$] (**A**), $H_2B{=}NMe_2$ (**B**), and [H_2BNMe_2]$_2$ (**C**) was observed at 298 K.

NMR data for *trans*-[Ir(H)(η^{1}-HBH$_2$·NMe$_2$H)PMe$_3$(^{t}Bu^{4}POCOP)][BAr$^{F}_4$] (3b). ^{1}H NMR (500.0 MHz, CD_2Cl_2, 193 K): δ 6.86 (t, $^{3}J_{H,H}$ = 7.8 Hz, 1H, 4-H), 6.50 (d, $^{3}J_{H,H}$ = 7.8 Hz, 2H, 3- and 5-H), 1.76 (d, PMe_3), 1.33 (BH_2 (terminal)), −10.20 (br s, 1H, Ir(η^{1}-HBH$_2$·NMe$_2$H)), −23.14 (q, $^{2}J_{H,P}$ = 15.0 Hz, 1H, Ir–H). The peak of ^{t}Bu protons could not be assigned as its peak overlapped with that of grease. The signal at 1.33 ppm for the B–$H_{terminal}$ hydrogen atoms of the co-ordinated borane could not be integrated as it overlapped with the signal of ^{t}Bu protons. ^{31}P{^{1}H} NMR (202.4 MHz, CD_2Cl_2, 193 K): δ 168.8 (br s, P(^{t}Bu)$_4$), −57.7 (br s, PMe_3). The peak of the bound $H_3B{\cdot}NMe_2H$ in complex **3b** was not characterized using ^{11}B NMR spectroscopy due to spectral broadening at low temperatures.

NMR data for [(NHMe$_2$)$_2$BH$_2$][BAr$^{F}_4$] (A). ^{11}B NMR (160.4 MHz, CD_2Cl_2, 298 K): δ −2.3 (br t, $^{1}J_{BH}$ = 115 Hz). ^{11}B{^{1}H} NMR (160.4 MHz, CD_2Cl_2, 298 K): δ −2.2 (br s).

NMR data for $H_2B{=}NMe_2$ (B). ^{11}B NMR (160.4 MHz, CD_2Cl_2, 298 K): δ 37.4 (br t, $^{1}J_{BH}$ = 126 Hz). ^{11}B{^{1}H} NMR (160.4 MHz, CD_2Cl_2, 298 K): δ 37.4 (br s).

NMR data for [H_2BNMe_2]$_2$ (C). ^{11}B NMR (160.4 MHz, CD_2Cl_2, 298 K): δ 5.1 (br t, $^{1}J_{BH}$ = 114 Hz). ^{11}B{^{1}H} NMR (160.4 MHz, CD_2Cl_2, 298 K): δ 5.1 (br s).

X-ray crystal structure analysis

X-ray diffraction intensity data were collected using a Bruker D8 Quest Photon-II diffractometer (3-axis goniometer with fixed Kappa geometry), equipped with graphite-monochromated Mo Kα radiation (λ = 0.71073 Å)[55] and an Oxford CryoSystem Plus Controller for low-temperature measurements (N_2 flow, 120 K). Data integration was performed using the Bruker SAINT software with a narrow-frame algorithm, and absorption corrections were applied *via* the SADABS multi-scan method.[56,57] The structure was solved using dual methods by SHELXT and refined by full-matrix least-squares on F^2 using SHELXL.[55–61] All non-hydrogen atoms were refined anisotropically. Hydrogen atoms bonded to carbon were positioned geometrically and refined using a riding model, with U_{eq} values set to 1.5× for terminal sp^3 and 1.2× for other C–H groups. The hydride hydrogen atom (H1) in [Ir(H)(PMe$_3$)(^{t}Bu^{4}POCOP)]$^{+}$ (**3**) (Fig. 2) was located from the difference Fourier map and refined freely (both its position and temperature factors were refined). Positional disorder was observed in two CF_3 groups (a common feature in weakly coordinating anions such as [BAr$^{F}_4$]$^{-}$)[62] and two *t*-butyl groups bonded to a phosphorus atom. These were modelled as two-component disorder, with each disordered atom assigned to two distinct positions with relative occupancies. Disordered groups were restrained to have similar geometries. U^{ij} components of ADPs for disordered atoms closer to each other than 1.7 Å were restrained to be similar. Disordered models of CF_3 were exported from the DSR[61] program onto the SHELXL instruction file. Molecular graphics were generated using ORTEP3 for Windows, and publication materials were prepared using SHELXLE and WinGX software packages.[57,58]

Computational details

All the geometrical optimisation in this study was performed with density functional theory (DFT), with the aid of the Turbomole 7.5 suite of programs,[63] using the PBE functional[64] and the def2-TZVP[65–67] basis set. The resolution of identity (RI),[68] along with the multipole accelerated resolution of identity (marij)[69] approximations, was employed for an accurate and effective treatment of the electronic Coulomb term in the DFT calculations. Solvent corrections were incorporated with optimisation calculations using the COSMO model,[70] with dichloromethane (ε = 8.93) as the solvent. We used Grimme's dispersion correction (DFT-D3)[71] to consider the long-range interactions. For further improvement, single-point calculations were carried out using the PBE0-D3/Def2-TZVP + COSMO (ε = 8.93) functional.[72] The values reported are ΔG values, with zero-point energy corrections, internal energy, and entropic contributions included through harmonic frequency calculations on the optimised minima, with the temperature set to 298.15 K. Harmonic frequency calculations were performed for all stationary points to confirm them as local minima. The absence of imaginary frequencies confirmed the minima, while the presence of a single imaginary frequency verified the transition states. Additionally, intrinsic reaction coordinate (IRC)[73] calculations were performed on transition states to further validate their authenticity and confirm the correct determination of reactant and product structures. Translational entropy values were corrected using the free volume correction introduced by Mammen *et al.*,[74] which is based on the Sackur–Tetrode equation. This correction provides a physically intuitive adjustment for the translational entropy of molecules in solution. The free energy profile is generated using MechaSVG.[75]

Author contributions

MP and BRJ planned the experiments. MP conducted all the experimental work. ZYS and KV performed the computational studies and AKP solved the X-ray crystal structure. BRJ planned the project and arranged funding.

Conflicts of interest

There are no conflicts to declare.

Data availability

The data supporting this article have been included as part of the supplementary information (SI). Supplementary information is available. See DOI: https://doi.org/10.1039/d5dt01780g.

CCDC 2464181 (**3**) contains the supplementary crystallographic data for this paper.[76]

Acknowledgements

MP and ZYS gratefully acknowledge UGC, India and UGC-NFSC, India for fellowships and IISc and CSIR-NCL for providing instrumental facilities. BRJ would like to thank SERB (CRG/2020/004769), India, for financial support.

References

1 G. J. Kubas, *Metal Dihydrogen and σ-Bond complexes*, Kluwer/Plenum, New York, 2001.
2 A. S. Weller, F. M. Chadwik and A. I. McKay, *Advances in Organometallic Chemistry*, Academic Press Inc., 2016, 66, 223–276.
3 C. Lenczyk, D. K. Roy, B. Ghosh, J. Schwarzmann, A. K. Phukan and H. Braunschweig, *Chem. – Eur. J.*, 2019, **25**, 8585–8589.
4 X. He and J. F. Hartwig, *J. Am. Chem. Soc.*, 1996, **118**, 1696–1702.
5 D. R. Lantero, D. L. Ward and M. R. Smith, *J. Am. Chem. Soc.*, 1997, **119**, 9699–9708.
6 G. Alcaraz and S. Sabo-Etienne, *Angew. Chem., Int. Ed.*, 2010, **49**, 7170–7179.
7 W. R. H. Wright, E. R. Berkeley, L. R. Alden, R. T. Baker and L. G. Sneddon, *Chem. Commun.*, 2011, **47**, 3177–3179.
8 V. Pons and R. T. Baker, *Angew. Chem., Int. Ed.*, 2008, **47**, 9600–9602.
9 A. Staubitz, A. P. M. Robertson and I. Manners, *Chem. Rev.*, 2010, **110**, 4079–4124.
10 J. R. Vance, A. Schäfer, A. P. M. Robertson, K. Lee, J. Turner, G. R. Whittell and I. Manners, *J. Am. Chem. Soc.*, 2014, **136**, 3048–3064.
11 C. E. Webster, Y. Fan, M. B. Hall, D. Kunz and J. F. Hartwig, *J. Am. Chem. Soc.*, 2003, **125**, 858–859.
12 G. M. Adams, A. L. Colebatch, J. T. Skornia, A. I. McKay, H. C. Johnson, G. C. Lloyd-Jones, S. A. Macgregor, N. A. Beattie and A. S. Weller, *J. Am. Chem. Soc.*, 2018, **140**, 1481–1495.
13 H. C. Johnson, C. L. McMullin, S. D. Pike, S. A. Macgregor and A. S. Weller, *Angew. Chem., Int. Ed.*, 2013, **52**, 9776–9780.
14 C. N. Brodie, L. Sotorrios, T. M. Boyd, S. A. Macgregor and A. S. Weller, *ACS Catal.*, 2022, **12**, 13050–13064.
15 M. Roselló-Merino, R. J. Rama, J. Díez and S. Conejero, *Chem. Commun.*, 2016, **52**, 8389–8392.
16 A. Ramaraj, H. K. Reddy, H. Keil, R. Herbst-Irmer, D. Stalke, E. D. Jemmis and B. R. Jagirdar, *Organometallics*, 2017, **36**, 2736–2745.
17 M. Shimoi, S. Nagai, M. Ichikawa, Y. Kawano, K. Katoh, M. Uruichi and H. Ogino, *J. Am. Chem. Soc.*, 1999, **121**, 11704–11712.
18 T. J. Hebden, M. C. Denney, V. Pons, P. M. B. Piccoli, T. F. Koetzle, A. J. Schultz, W. Kaminsky, K. I. Goldberg and D. M. Heinekey, *J. Am. Chem. Soc.*, 2008, **130**, 10812–10820.

19 J. Choi, N. E. Schloerer, J. Berger and M. H. G. Prechtl, *Dalton Trans.*, 2014, **43**, 290–299.
20 A. Kumar, J. S. A. Ishibashi, T. N. Hooper, T. C. Mikulas, D. A. Dixon, S.-Y. Liu and A. S. Weller, *Chem. – Eur. J.*, 2016, **22**, 310–322.
21 M. J. Cross, C. N. Brodie, D. G. Crivoi, J. C. Goodall, D. E. Ryan, A. J. Martínez-Martínez, A. Johnson and A. S. Weller, *Chem. – Eur. J.*, 2023, **29**, e202302110.
22 H. C. Johnson, A. P. M. Robertson, A. B. Chaplin, L. J. Sewell, A. L. Thompson, M. F. Haddow, I. Manners and A. S. Weller, *J. Am. Chem. Soc.*, 2011, **133**, 11076–11079.
23 M. C. Denney, V. Pons, T. J. Hebden, D. M. Heinekey and K. I. Goldberg, *J. Am. Chem. Soc.*, 2006, **128**, 12048–12049.
24 A. Staubitz, M. E. Sloan, A. P. M. Robertson, A. Friedrich, S. Schneider, P. J. Gates, J. S. A. D. Günne and I. Manners, *J. Am. Chem. Soc.*, 2010, **132**, 13332.
25 A. Rossin and M. Peruzzini, *Chem. Rev.*, 2016, **116**, 8848–8872.
26 R. Kumar and B. R. Jagirdar, *Inorg. Chem.*, 2013, **52**, 28–36.
27 H. C. Johnson, E. M. Leitao, G. R. Whittell, I. Manners, G. C. Lloyd-Jones and A. S. Weller, *J. Am. Chem. Soc.*, 2014, **136**, 9078–9093.
28 G. Algarra, L. J. Sewell, H. C. Johnson, S. A. Macgregor and A. S. Weller, *Dalton Trans.*, 2014, **43**, 11118–11128.
29 S. Chakraborty, J. Zhang, Y. J. Patel, J. A. Krause and H. Guan, *Inorg. Chem.*, 2013, **52**, 37–47.
30 S. Murugesan, B. Stöger, M. Weil, L. F. Veiros and K. Kirchner, *Organometallics*, 2015, **34**, 1364–1372.
31 S. Selvarasu, G. Joshi, D. Senthurpandi, M. Nethaji, E. D. Jemmis and B. R. Jagirdar, *Organometallics*, 2024, **43**, 2755–2766.
32 Z. Mo, Y. Liu and L. Deng, *Angew. Chem., Int. Ed.*, 2013, **52**, 10845–10849.
33 S. Zhang, X. Zhai, Y. Song, L. Feng, C.-H. Tung and W. Wang, *Organometallics*, 2021, **40**, 1692–1698.
34 N. K. Agrawal, S. R. Dash, K. Vanka, M. Nethaji and B. R. Jagirdar, *J. Organomet. Chem.*, 2022, **965–966**, 122317.
35 J. Yang and M. Brookhart, *J. Am. Chem. Soc.*, 2007, **129**, 12656–12657.
36 A. D. R. Shada, A. J. M. Miller, T. J. Emge and A. S. Goldman, *ACS Catal.*, 2021, **11**, 3009–3016.
37 N. K. Agrawal, S. R. Dash, K. Vanka and B. R. Jagirdar, *Organometallics*, 2023, **42**, 441–456.
38 D. B. Lao, A. C. E. Owens, D. M. Heinekey and K. I. Goldberg, *ACS Catal.*, 2013, **3**, 2391–2396.
39 J. Yang and M. Brookhart, *J. Am. Chem. Soc.*, 2007, **129**, 12656–12657.
40 J. M. Goldberg, G. W. Wong, K. E. Brastow, W. Kaminsky, K. I. Goldberg and D. M. Heinekey, *Organometallics*, 2015, **34**, 753–762.
41 J. M. Goldberg, K. I. Goldberg, D. M. Heinekey, S. A. Burgess, D. B. Lao and J. C. Linehan, *J. Am. Chem. Soc.*, 2017, **139**, 12638–12646.
42 J. M. Goldberg, S. D. T. Cherry, L. M. Guard, W. Kaminsky, K. I. Goldberg and D. M. Heinekey, *Organometallics*, 2016, **35**, 3546–3556.
43 F. A. Jalón, A. Otero, B. R. Manzano, E. Villaseñor and B. Chaudret, *J. Am. Chem. Soc.*, 1995, **117**, 10123–10124.
44 S. Sabo-Etienne, B. Chaudret, H. A. Makarim, J. C. Barthelat, J. P. Daudey, S. Ulrich, H. H. Limbach and C. Moise, *J. Am. Chem. Soc.*, 1995, **117**, 11602–11603.
45 S. Shafiei-Haghighi, L. M. Singer, S. R. Tamang and M. Findlater, *Polyhedron*, 2018, **143**, 126–131.
46 S. G. Shore, C. W. Hickam Jr. and D. Cowles, *J. Am. Chem. Soc.*, 1965, **87**, 2755–2756.
47 S. Pal, S. Kusumoto and K. Nozaki, *Organometallics*, 2018, **37**, 906–914.
48 M. Roselló-Merino, J. López-Serrano and S. Conejero, *J. Am. Chem. Soc.*, 2013, **135**, 10910–10913.
49 E. M. Titova, E. S. Osipova, A. A. Pavlov, O. A. Filippov, S. V. Safronov, E. S. Shubina and N. V. Belkova, *ACS Catal.*, 2017, **7**, 2325–2333.
50 C. H. Li and T. D. Stewart, *J. Am. Chem. Soc.*, 1937, **59**, 2596–2599.
51 E. A. K. Spearing-Ewyn, N. A. Beattie, A. L. Colebatch, A. J. Martinez-Martinez, A. Docker, T. M. Boyd, G. Baillie, R. Reed, S. A. Macgregor and A. S. Weller, *Dalton Trans.*, 2019, **48**, 14724–14736.
52 K. Fujiwara, S. Yasuda and T. Mizuta, *Organometallics*, 2014, **33**, 6692–6695.
53 J. L. Herde, J. C. Lambert, C. V. Senoff and M. A. Cushing, *Inorg. Synth.*, 1974, **15**, 19–20.
54 I. Göttker-Schnetmann, P. White and M. Brookhart, *J. Am. Chem. Soc.*, 2004, **126**, 1804–1811.
55 Bruker, *D8 QUEST*, Bruker AXS Inc., Madison, Wisconsin, USA, 2012.
56 Bruker, *SAINT*, Bruker AXS Inc., Madison, Wisconsin, USA, 2012.
57 L. J. Farrugia, *J. Appl. Crystallogr.*, 2012, **45**, 849–854.
58 C. B. Hübschle, G. M. Sheldrick and B. Dittrich, *J. Appl. Crystallogr.*, 2011, **44**, 1281–1284.
59 G. M. Sheldrick, *Acta Crystallogr., Sect. C: Struct. Chem.*, 2015, **71**, 3–8.
60 G. M. Sheldrick, *Acta Crystallogr., Sect. A: Found. Adv.*, 2015, **71**, 3–8.
61 D. Kratzert, J. J. Holstein and I. Krossing, *J. Appl. Crystallogr.*, 2015, **48**, 933–938.
62 A. B. Chaplin and A. S. Weller, *Eur. J. Inorg. Chem.*, 2010, 5124–5128, DOI: 10.1002/ejic.201000686.
63 TURBOMOLE V7.5 2020, a development of University of Karlsruhe and Forschungszentrum Karlsruhe GmbH, 1989–2007, TURBOMOLE GmbH, since 2007; available from https://www.turbomole.org.
64 J. P. Perdew, K. Burke and M. Ernzerhof, *Phys. Rev. Lett.*, 1996, **77**, 3865–3869.
65 A. Schäfer, C. Huber and R. Ahlrichs, *J. Chem. Phys.*, 1994, **100**, 5829–5835.
66 F. Weigend and R. Ahlrichs, *Phys. Chem. Chem. Phys.*, 2005, **7**, 3297–3305.
67 F. Weigend, *Phys. Chem. Chem. Phys.*, 2006, **8**, 1057–1065.
68 K. Eichkorn, O. Treutler, H. Öhm, M. Häser and R. Ahlrichs, *Chem. Phys. Lett.*, 1995, **240**, 283–290.

69 M. Sierka, A. Hogekamp and R. Ahlrichs, *J. Chem. Phys.*, 2003, **118**, 9136–9148.
70 A. Klamt and G. Schüürmann, *J. Chem. Soc., Perkin Trans. 2*, 1993, 799–805.
71 S. Grimme, J. Antony, S. Ehrlich and H. Krieg, *J. Chem. Phys.*, 2010, **132**, 154104.
72 C. Adamo and V. Barone, *J. Chem. Phys.*, 1999, **110**, 6158–6170.
73 K. Fukui, *Acc. Chem. Res.*, 1981, **14**, 363.
74 M. Mammen, E. I. Shakhnovich, J. M. Deutch and G. M. Whitesides, *J. Org. Chem.*, 1998, **63**, 3821–3830.
75 R. A. Angnes, *mechaSVG*, GitHub repository, 2020. DOI: 10.5281/zenodo.4065333.
76 CCDC 2464181: Experimental Crystal Structure Determination, 2025, DOI: 10.5517/ccdc.csd.cc2nq5q9.